

Probabilistic Forecasting of the Arctic Sea Ice Edge with Contour Modeling¹

Hannah M. Director
Department of Statistics
University of Washington

Adrian E. Raftery
Departments of Statistics and Sociology
University of Washington

Cecilia M. Bitz
Department of Atmospheric Sciences
University of Washington

April 8, 2024

¹The authors thank Nicholas Wayand for assistance with data processing and Arlan Dirkson for addressing questions on Trend Adjusted Quantile Mapping. Any opinions, findings, and conclusions or recommendations expressed in this material are those of the authors and do not necessarily reflect the views of the National Science Foundation. Results in this paper were produced using the *IceCast* R package (Director et al., 2020). Relevant code can also be accessed at <https://github.com/hdirector/ProbSeaIce>.

Abstract

Sea ice, or frozen ocean water, freezes and melts every year in the Arctic. Forecasts of where sea ice will be located weeks to months in advance have become more important as the amount of sea ice declines due to climate change, for maritime planning and other uses. Typical sea ice forecasts are made with ensemble models, physics-based models of sea ice and the surrounding ocean and atmosphere. This paper introduces Mixture Contour Forecasting, a method to forecast sea ice probabilistically using a mixture of two distributions, one based on post-processed output from ensembles and the other on observed sea ice patterns in recent years. At short lead times, these forecasts are better calibrated than unadjusted dynamic ensemble forecasts and other statistical reference forecasts. To produce these forecasts, a statistical technique is introduced that directly models the sea ice edge contour, the boundary around the region that is ice-covered. Mixture Contour Forecasting and reference methods are evaluated for monthly sea ice forecasts for 2008-2016 at lead times ranging from 0.5-6.5 months using one of the European Centre for Medium-Range Weather Forecasts ensembles.

Keywords: spatiotemporal, climate change, forecasting, post-processing, mixtures.

Contents

1	Introduction	1
2	Contour model	2
2.1	Notation and setup	3
2.2	Statistical model	6
2.3	Parametric covariance	8
2.4	Number of lines	9
2.5	Prior distribution of the mean sea ice edge	9
2.5.1	Contour-Shifting	9
2.5.2	Prior for mean proportions ice-covered	10
2.6	Prior for Covariance	11
2.7	Posterior distribution	12
2.8	Model fitting	13
3	Mixture Contour Forecasting	14
4	Method evaluation	15
4.1	Model outputs and observations	15
4.2	Reference forecasts	17
4.3	Visualizing forecasts	18
4.4	Assessing Calibration	20
4.5	Assessing accuracy	20
4.6	Binary Forecasts	21
4.7	Understanding mixture weights	23
5	Discussion	23
A	Standard deviation corresponding to γ proportion of mass of a Gaussian within symmetric bounds	30
B	Additional figures	30
C	MCMC diagnostics	35
C.1	Example Evaluation: September 2005, 1.5-month lead	35
D	Length of Training Periods	40

List of Tables

1	Summary of forecast types evaluated. Probabilistic forecasts give estimates in the interval $[0, 1]$ and binary forecasts indicate predicted sea ice presence	17
2	The 50-th, 95-th, and 100-th percentile for the estimated chain lengths for μ_i obtained from the Raftery and Lewis Diagnostic for the three regions evaluated. Values rounded to the nearest whole number.	36
3	As in Table 2, except for σ_i	36
4	Estimated chain lengths from the Raftery and Lewis Diagnostic for κ	36
5	Mean area-weighted Brier scores for MCF on the test set of 2012-2016 for different numbers of years of training data used to determine the weight on the climatology versus the contour model forecast.	41

List of Figures

1	The average proportion of times sea ice was present, plotted against the predicted probability of sea ice presence for the unadjusted ECMWF ensemble forecasts (left) and for the corresponding Mixture Contour Forecasts (right) for lead times of 0.5 to 1.5 months. Results are for September 2008-2016. A perfectly calibrated forecast would have all points on the $y = x$ line, so the MCF method forecast is better calibrated.	3
2	Arctic ocean regions used here. Each region in a color other than beige is fit with a contour model. The bold lines in all regions except the Central Arctic are the lines from which the fixed set of boundary points \mathbf{B} are drawn. The boundary points themselves are plotted on top of these lines. The ‘+’ symbol denotes the location of \mathbf{B} in the Central Arctic Region. Areas in grey are land and areas in white are ocean regions that are not considered part of the Arctic ocean in the National Snow and Ice Data Center land mask (National Snow and Ice Data Center, 2017).	4
3	Hypothetical sea ice edge contours (\mathbf{S}), sets of fixed boundary points (\mathbf{B}), and parallel lines (\mathbf{L}) on which the points $\tilde{\mathbf{S}}$ will be generated for a sample typical region (left) and for the Central Arctic region (right). The green line designates the observed ice-covered line segments for the 14th (left) and 33rd (right) lines.	5
4	Illustration of a hypothetical line segment, L_i that crosses over multiple sections of land. Line L_i starts at point B_i , denoted by a ‘+’ sign, and ends at the black circle. The j -th line segment crossing ocean in L_i is denoted by $R_{i,j}$ and the j -th line segment crossing land is denoted by $H_{i,j}$. There are K_i sections crossing ocean and $K_i - 1$ sections crossing land.	6
5	Forecasts of the probability of sea ice presence for September 2008 using different methods. The forecasts are described in Table 1. The red line is the observed sea ice edge contour and grey areas are land. For MCF, the observed ice edge is almost completely within areas with positive probability and has little area where sea ice is was predicted with probability 1 but sea ice was not present in observations. In contrast, the observed sea ice edge more often goes through regions with zero probability in the ensemble and climatology forecasts. In the climatology forecast, there is also the most area where sea ice is predicted with probability 1 but is not present in observations.	19

6	The average proportion of the time sea ice was present plotted against the predicted probability of sea ice presence for the raw ECMWF forecasts (left), after post-processing with MCF (middle), and TAQM (right). Forecasts are grouped into lead times of 0.5 and 1.5 months (top) and 2.5-6.5 months (bottom). A perfectly calibrated forecast would have all points on the diagonal $y = x$ line.	21
7	Top: Average Brier scores by month for the test years 2008-2016 for the probabilistic forecasts. The Brier Score for each grid box is weighted based on its area. Forecasts are described in Table 1. Bottom: As above, but for the binary forecasts.	22
8	Weight on the contour model by month and lead time. A black dot indicates that the weight is at least 0.4. The contour gets more weight at short lead times and in months near the sea ice minimum. The weight on climatology is equal to one minus the weight on the contour model.	23
9	Overall Brier scores for the test years 2008-2016 for the probabilistic forecasts and a damped persistence reference binary forecast. The Brier Score for each grid box is weighted based on its area. Forecasts are described in Table 1 in the main text. . . .	31
10	Average Brier scores grouped into three-month sets for the test years 2008-2016 for the probabilistic forecasts and a damped persistence reference binary forecast. The Brier Score for each grid box is weighted based on its area. Forecasts are described in Table 1 in the main text.	31
11	As in Figure 10, except for binary forecasts.	32
12	Plots of the average proportion of times sea ice was present against the predicted probability of sea ice presence for the raw ECMWF (top), MCF (middle), and TAQM (bottom) forecasts for lead times of 0.5 - 1.5 months. Results are grouped into three-month sets and all grid boxes are equally weighted.	33
13	As in Figure 12 but for lead times of 2.5 - 6.5 months.	34
14	Traceplots for the chains in each of the three evaluated regions for a typical μ_i . . .	37
15	Traceplots for the chains in each of the three evaluated regions for a typical σ_i . . .	38
16	Traceplots for the parameter κ in the three evaluated regions.	39

1 Introduction

Sea ice, or frozen ocean water, freezes and melts annually in response to seasonal changes in atmospheric and oceanic processes. Since the satellite record began in 1979, the amount of sea ice in the Arctic has declined rapidly (Comiso et al., 2008; Stroeve et al., 2012). Continued reduction in sea ice is expected as the effects of climate changes increase. Reduced sea ice cover allows for increased Arctic shipping (Smith and Stephenson, 2013; Melia et al., 2016). The importance of forecasting sea ice has increased in response, since waters without sea ice are more easily navigable than waters with sea ice. Reliable estimates of a ship’s probability of encountering sea ice are needed to plan maritime routes that avoid sea ice. In this paper, we develop statistical methods to accurately predict the probability of encountering sea ice.

Sea ice concentration, or the percent of ice-covered area, has been derived from satellite measurements for a little over 40 years and is reported on a grid. For navigational purposes, the concentration field can be reduced to a binary field indicating the presence or absence of sea ice. Prediction efforts then focus on the location of the ice edge contour, or the boundary line that separates ice-covered regions and open water. We follow the convention in sea ice research of categorizing a grid box as ice-covered if its concentration is at least 15%. Thresholding is needed, since satellites often fail to distinguish between areas of open water and areas where water is melting on the sea ice’s surface. Concentration reduces from about 50% to near 0% concentration over a small region, so the area classified as sea ice is only weakly affected by the exact threshold concentration used.

Zhang and Cressie (2019, 2020) have introduced hierarchical spatio-temporal generalized linear models for Arctic sea ice. However, many sea ice forecasts used in practice are informed by numerical prediction systems. These systems integrate systems of differential equations to represent the physical processes that drive sea ice formation and melting. These systems are typically run multiple times with slightly different initial conditions, and the outputs from the resulting runs have varying amounts of sea ice. The collection of forecasts, referred to as the ensemble, has shown skill in predicting the total area or extent of sea ice at seasonal time scales in retrospective forecasts (e.g., Sigmond et al., 2013; Msadek et al., 2014; Wang et al., 2013; Chevallier et al., 2013) and in current forecasts (Blanchard-Wrigglesworth et al., 2015). Skill has also been shown at regional scales (Bushuk et al., 2017) and for spatial fields for some models at short lead times (Zampieri et al., 2018).

However, errors in ensembles are common because the underlying systems of differential equations are only approximations of the true physical processes, because initial conditions are not fully known, and because of sub-grid scale phenomena (Guemas et al., 2016; Blanchard-Wrigglesworth et al., 2015). An ensemble can be biased, meaning that its mean

behavior is systematically incorrect. It can also be poorly calibrated, meaning that the range of possible sea ice states predicted by the ensemble members does not reflect the actual uncertainty of the forecast.

Statistical post-processing, or methods that incorporate or adjust information from ensemble forecasts, can be applied to address ensembles’ weaknesses while maintaining much of the skill they provide. In this paper, we develop Mixture Contour Forecasting (MCF), a post-processing method to improve the calibration of sea ice forecasts. First, a method for generating distributions of sea ice edge contours is developed. The mean location of the sea ice edge contour in these distributions is partially informed by the mean location of the sea ice edge contour obtained from ensemble outputs. The forecasts obtained from these generated contour distributions are then weighted with climatological information to account for the time-varying skill of ensemble forecasts and aspects of sea ice that cannot be represented well with a contour boundary, such as holes in the sea ice.

The MCF method provides better calibrated and more accurate probabilistic forecasts than the unadjusted ensemble and better calibrated forecasts than existing post-processing techniques. In Figure 1, we illustrate the extent to which MCF improves model calibration by plotting the predicted probability of sea ice presence in September against the actual proportion of times sea ice was observed for the raw ensemble and after post-processing. The predictions are from the fifth generation of the European Centre for Medium-Range Weather Forecasts (ECMWF) seasonal forecasting season (SEAS5) (Johnson et al., 2019; European Centre for Medium-Range Weather Forecasts, 2017). We see that MCF provides much improved model calibration.

The paper is organized as follows. In Section 2, we introduce a Bayesian model for generating distributions of the sea ice edge contour. This contour model is fit to observed ice edge contours from recent years and its prior is partially informed from the mean ice edge predicted from a dynamic ensemble. In Section 3, the contour model is combined with climatological information using a finite mixture model. In Section 4, we compare the performance of MCF to other post-processing and statistical forecasting techniques. In Section 5, we conclude with discussion.

2 Contour model

In this section, we develop a Bayesian model for the distribution of sea ice edge contours. The method works by directly modeling contours as a sequence of connected points.

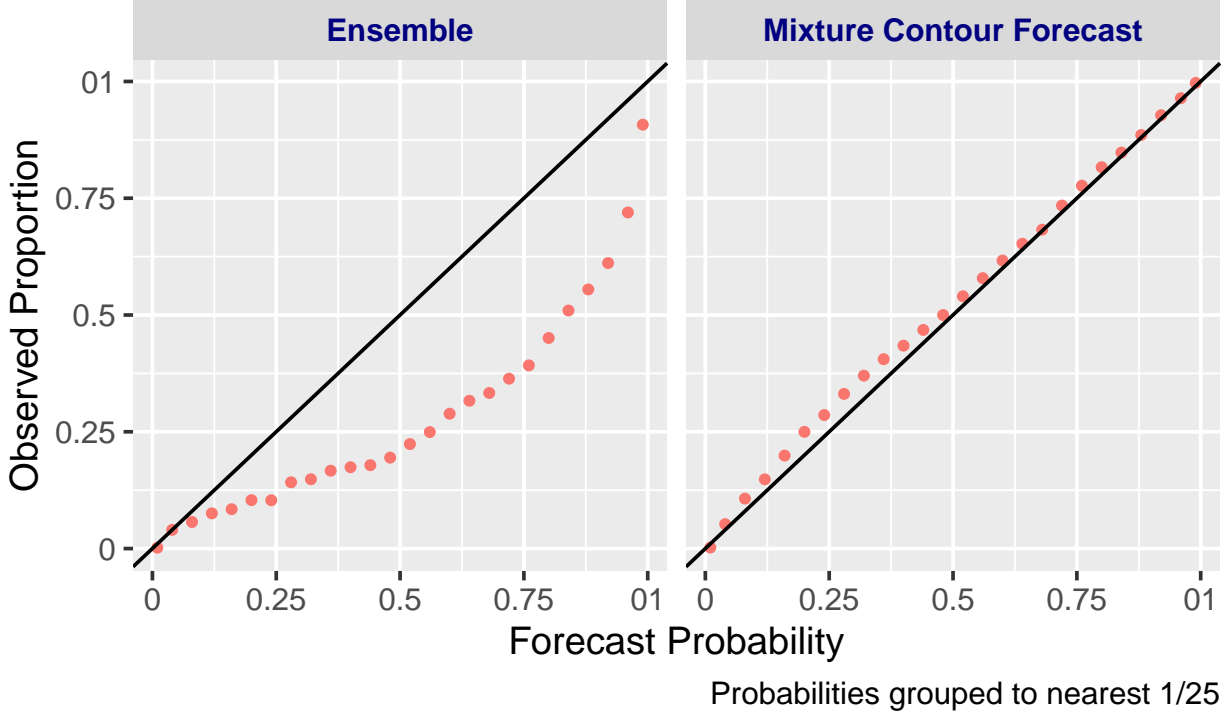


Figure 1: The average proportion of times sea ice was present, plotted against the predicted probability of sea ice presence for the unadjusted ECMWF ensemble forecasts (left) and for the corresponding Mixture Contour Forecasts (right) for lead times of 0.5 to 1.5 months. Results are for September 2008-2016. A perfectly calibrated forecast would have all points on the $y = x$ line, so the MCF method forecast is better calibrated.

2.1 Notation and setup

A contour is the boundary line enclosing a defined area, which in this case is the region that contains sea ice. A contour, denoted by \mathbf{S} , can be represented as an ordered sequence of N spatial points, (S_1, \dots, S_N) , where each S_i is an (x, y) coordinate pair. Connecting S_i to S_{i+1} for all $i = 1, \dots, N - 1$ and S_N to S_1 encloses an area. Following this definition, to generate a distribution of contours we need a way to generate realizations of \mathbf{S} .

While the sea ice edge is often referred to as a single entity, it is actually a collection of edges defining multiple contiguous areas of sea ice. As such, it is natural to model multiple contours separately. We focus on five regions individually. These five regions, shown in the map in Figure 2, exclude parts of the Arctic ocean where a contour model is not appropriate because the sea ice does not typically form one contiguous section. We selected these regions by modifying an existing region mask (Cavalieri and Parkinson, 2012) obtained from the National Snow and Ice Data Center (2017). For notational simplicity, we do not subscript the regions and refer to the sea ice edge contour in a given region simply as \mathbf{S} .



Figure 2: Arctic ocean regions used here. Each region in a color other than beige is fit with a contour model. The bold lines in all regions except the Central Arctic are the lines from which the fixed set of boundary points \mathbf{B} are drawn. The boundary points themselves are plotted on top of these lines. The ‘+’ symbol denotes the location of \mathbf{B} in the Central Arctic Region. Areas in grey are land and areas in white are ocean regions that are not considered part of the Arctic ocean in the National Snow and Ice Data Center land mask (National Snow and Ice Data Center, 2017).

In most regions, sea ice is formed in contiguous sections bordering land. In these regions, \mathbf{S} is formed by a sequence of points that proceed from the coastline, into the ocean, and back to the coastline. We can reduce the number of points that need to be estimated by fixing a set of boundary points, $\mathbf{B} = (B_1, \dots, B_n)$, on land and considering how far into the ocean the contour extends at each boundary location. The subset of points in \mathbf{S} which must be fit are denoted by $\tilde{\mathbf{S}}$ and are indexed $\{1, 2, \dots, n\}$. We lay out an ordered series of parallel lines, $\mathbf{L} = (L_1, \dots, L_n)$, that cover the region. Each L_i extends from its corresponding point B_i to the edge of the region. We assume that one point, \tilde{S}_i , lies on each line, L_i . We denote the line segment from each point on the coastline, B_i , to the corresponding point \tilde{S}_i as y_i . The set of all line segments is denoted by $\mathbf{Y} = (y_1, \dots, y_n)$. The contour is then formed by connecting the points B_i to B_{i+1} for all $i = 1, \dots, n - 1$, B_n to \tilde{S}_n , \tilde{S}_i to \tilde{S}_{i-1} for all

$i = n, \dots, 2$, and \tilde{S}_1 to B_1 . The left panel of Figure 3 illustrates these values for the Bering Sea. The angle of all lines in \mathbf{L} is set to approximately match the direction the sea ice grows off the land in each region.

Unlike in other regions, sea ice in the Central Arctic region is not generally formed off a land boundary. To represent the Central Arctic's contour, we fix all the lines in \mathbf{L} to originate from a single fixed central point rather than from a sequence of points. So, for this region $B_i = B_j$ for all $B_i, B_j \in \mathbf{B}$. The lines extend at fixed angles evenly spaced around a circle as illustrated in the right panel of Figure 3. In this case, $\tilde{\mathbf{S}} = \mathbf{S}$ and $n = N$.

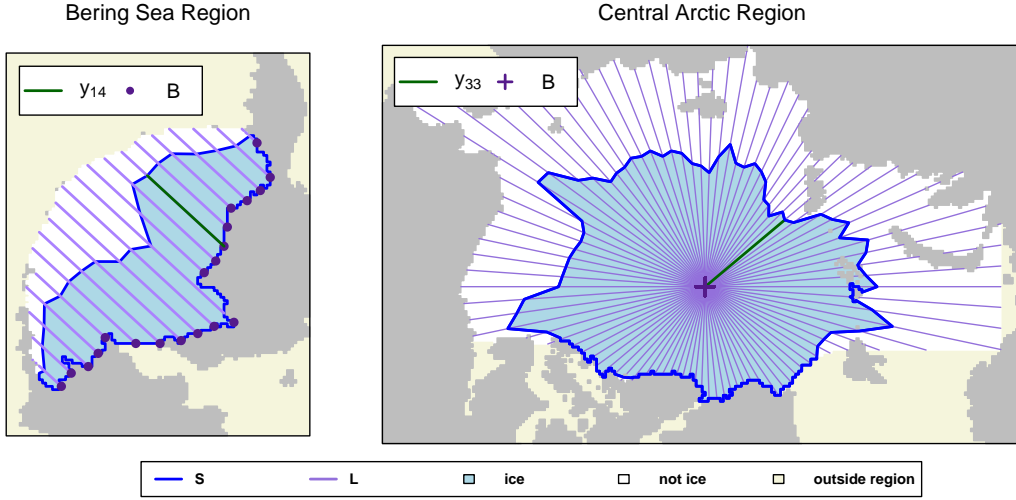


Figure 3: Hypothetical sea ice edge contours (\mathbf{S}), sets of fixed boundary points (\mathbf{B}), and parallel lines (\mathbf{L}) on which the points $\tilde{\mathbf{S}}$ will be generated for a sample typical region (left) and for the Central Arctic region (right). The green line designates the observed ice-covered line segments for the 14th (left) and 33rd (right) lines.

Note that given \mathbf{B} , \mathbf{Y} , and the angles of all lines in \mathbf{L} , we have enough information to identify each \tilde{S}_i . We need only compute the length of each line segment $y_i \in \mathbf{Y}$. Each coordinate of the contour is then,

$$\tilde{s}_i = \mathbf{B}_i + (||y_i|| \cos(\theta_i), ||y_i|| \sin(\theta_i)) \quad (1)$$

where $||\cdot||$ denotes the length of line segment and θ_i is the angle of line L_i . Therefore, to generate distributions of contours, we need only develop a statistical model for generating the length of the line segments in \mathbf{Y} , since \mathbf{B} and \mathbf{L} are fixed.

2.2 Statistical model

For the sea ice application, each line L_i is bounded below by zero and above by land and regions boundaries. Additionally, some L_i cross over land sections, where sea ice cannot be observed. These constraints make it natural to model the proportion of each line that is ice-covered, rather than model the length of the line segments that compose \mathbf{Y} directly.

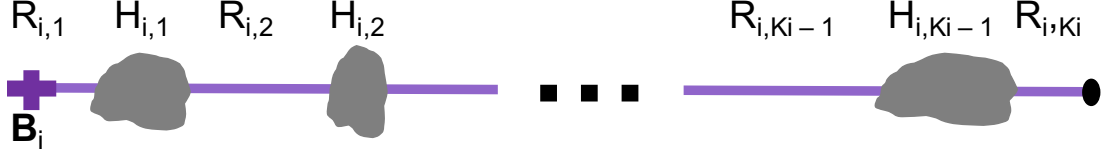


Figure 4: Illustration of a hypothetical line segment, L_i that crosses over multiple sections of land. Line L_i starts at point B_i , denoted by a ‘+’ sign, and ends at the black circle. The j -th line segment crossing ocean in L_i is denoted by $R_{i,j}$ and the j -th line segment crossing land is denoted by $H_{i,j}$. There are K_i sections crossing ocean and $K_i - 1$ sections crossing land.

We now introduce notation for modeling proportions. These variables are illustrated in Figure 4. Let $\mathbf{R}_i = \{R_{i,1}, \dots, R_{i,K_i}\}$ denote the K_i line segments that form L_i and let $\mathbf{H}_i = \{H_{i,1}, \dots, H_{i,K_i-1}\}$ denote the $K_i - 1$ line segments where land is crossed. Note that

$$\|L_i\| = \sum_{k=1}^{K_i} \|R_{i,k}\| + \sum_{k=1}^{K_i-1} \|H_{i,k}\| = \|\mathbf{R}_i\| + \|\mathbf{H}_i\|. \quad (2)$$

In the common case where L_i just goes through ocean, $\mathbf{R} = R_{i1} = L_i$ and $\mathbf{H} = \emptyset$.

Since the line segments forming any H_i cannot contain sea ice, we focus on modeling the proportion of the corresponding R_i that are ice-covered. More formally, let

$$\pi_i = \frac{\|y_i \cap \mathbf{R}_i\|}{\|\mathbf{R}_i\|}, \quad (3)$$

where the numerator denotes the length of y_i that intersects the ocean line segments and the dominator denotes the total length of of ocean line segments in L_i . The set of all proportions is denoted by $\boldsymbol{\pi} = (\pi_1, \dots, \pi_n)$.

We develop a model for $\boldsymbol{\pi}$ that can be used to generate \mathbf{Y} and corresponding $\tilde{\mathbf{S}}$. For ease of modeling, we transform the proportions to the real line. Let

$$\tilde{\pi}_i = \begin{cases} \text{logit}(\pi_i) & \text{for } \epsilon \leq \pi_i \leq 1 - \epsilon \\ \text{logit}(\epsilon) & \text{for } \pi_i < \epsilon \\ \text{logit}(1 - \epsilon) & \text{for } \pi_i > 1 - \epsilon, \end{cases} \quad (4)$$

where $\text{logit}(x) = \log(x/(1-x))$ and ϵ is small. In our implementation $\epsilon = 0.01$. The set of transformed proportions, $\tilde{\boldsymbol{\pi}}$, are modeled using a multivariate normal distribution,

$$\tilde{\boldsymbol{\pi}} \sim N(\boldsymbol{\mu}, \boldsymbol{\Sigma}). \quad (5)$$

where $\boldsymbol{\mu}$ is an $n \times 1$ mean vector and $\boldsymbol{\Sigma}$ is an $n \times n$ covariance matrix.

The data generating process for $\tilde{\boldsymbol{S}}$ is then as follows. First an underlying random vector, $\tilde{\boldsymbol{\pi}}$, is drawn, Then each $\tilde{\pi}_i$ is transformed back to a proportion via

$$\pi_i = \text{ilogit}(\tilde{\pi}_i), \quad (6)$$

where $\text{ilogit}(x) = \exp(x)/(1 + \exp(x))$. The length of the corresponding y_i can be computed from π_i as follows. Let D denote the maximum index of a line segment of R_i that is fully ice-covered when a proportion π_i of \mathbf{R}_i is ice-covered:

$$D = \underset{d}{\text{argmin}} \left\{ \frac{\sum_{k=1}^d \|R_{i,k}\|}{\|\mathbf{R}_i\|} < \pi_i \right\}. \quad (7)$$

Then, the length of y_i is

$$\|y_i\| = \pi_i \|\mathbf{R}_i\| + \sum_{k=1}^{D-1} \|H_{i,k}\|. \quad (8)$$

In other words, y_i is composed of a proportion π_i of \mathbf{R}_i and all the line segments of \mathbf{H}_i that must be crossed to reach the D -th segment of \mathbf{R}_i . For all i , the lengths of y_i are then used to compute \mathbf{s}_i using Equation 1. Connecting the points in $\tilde{\boldsymbol{S}}$, along with the points in \mathbf{B} , if applicable, produces a generated contour.

In rare cases, the generated values in $\tilde{\boldsymbol{S}}$ will result in a contour that intersects itself. When these self-intersections occur, the contour fails to be a boundary around a single contiguous area. In such cases, a small adjustment is made with the Douglas-Peucker algorithm to the part(s) of the contours that have self-intersections. The Douglas-Peucker algorithm takes as input a line represented as a connected sequence of points and returns a new line that approximates the original line with a different connected sequence of points. The new line uses as few points as possible to approximate the old line while ensuring that the new line differs from the old line by no more than a distance of η (Douglas and Peucker, 1973). To correct self-intersections, the Douglas-Peucker algorithm is initially applied with a small η to the part of a contour with a self-intersection. If the self-intersection is removed, the new line is used in place of the old line. If not, η is increased and the algorithm is reapplied. This process is repeated until an η is found that produces a contour with no self-intersections. In our context, these adjustments typically have minimal effect on the line itself and the area contained within the contour.

We also adjust a small percent of generated $\|y_i\|$ values that correspond to locations where the generated contour is very close to touching a region boundary or land (within 12.5 nominal kilometers, or half the nominal length of a grid box). In such cases, our statistical model is predicting that the contour comes very close to, but does not actually touch, a land or region boundary. This behavior is physically implausible near land, so we adjust these $\|y_i\|$ values to exactly align with the region or land boundary. The total area involved in this adjustments is very small. This step ensures that any individual generated contour looks physically realistic.

2.3 Parametric covariance

To allow for efficient fitting of Equation 5, we define a parametric covariance structure. In sea ice observations, the mean and covariance of the ice-covered proportion of each line varies substantially within and across regions. To represent these features well, we need a statistical model with a reasonably flexible covariance structure. The values of $\tilde{\pi}_i$ and $\tilde{\pi}_j$ tend to be more similar when L_i and L_j are close together. So, we structure our covariance in all regions except the Central Arctic based on the differences between the indices of the lines in \mathbf{L} .

Outside the Central Arctic, we let $\Sigma = \Sigma(\boldsymbol{\sigma}, \kappa)$ where $\boldsymbol{\sigma} = (\sigma_1, \dots, \sigma_n)$ and $\kappa > 0$. The element, Σ_{ij} , in the i -th row and j -th column of this covariance is

$$\Sigma_{ij} = \sigma_i \sigma_j \exp \left(-\frac{|i - j|}{\kappa} \right). \quad (9)$$

where $|\cdot|$ denotes the absolute value.

In the Central Arctic region, the lines are laid out in a circle so that the first and last lines are close to each other despite their indices being far apart. Then the difference between the indices of line i and line j does not correspond to the distance between lines L_i and L_j . So we apply an alternative covariance function based on the difference between angles θ_i and θ_j . Various covariance functions based on differences between angles have been proposed (Gneiting, 2013). Like the other regions, we apply an exponential covariance structure where $\boldsymbol{\sigma} = (\sigma_1, \dots, \sigma_n)$, $\kappa > 0$, and the element in the i -th row and j -th column of the covariance matrix is

$$\Sigma_{ij} = \sigma_i \sigma_j \exp \left(-\frac{d(\theta_i, \theta_j)}{\kappa} \right), \quad (10)$$

where $d(\theta_i, \theta_j) \in [0, \pi]$ is the smaller angle between θ_i and θ_j .

We find that an exponential covariance structure fits the data well. In particular, this covariance structure allows for the correlation to drop off rapidly as lines become farther apart, while maintaining some non-zero correlation among all lines. Allowing for the latter

behavior is needed, since some region-wide correlation would be expected given large-scale phenomena that could occur across a region, such as a particularly cold or warm month.

2.4 Number of lines

Setting N , the number of lines in \mathbf{L} , involves tradeoffs between accuracy and computation time. With more lines, contours can be represented in more detail. However, computation increases with the corresponding increase in the size of the covariance matrix. Insight into this tradeoff can be obtained by considering how well a set of observed contours can be approximated with only points on lines in \mathbf{L} . The mean difference in area between observed contours and their approximations provides an estimate of the expected area that a generated contour built with N lines cannot represent.

In this implementation, we set N based on observations of the largest region (the Central Arctic) in the forecast month with the highest variability (September). Using data from 1995-2004, we find that approximating the observed September contours with points on $N = 90$ lines results in area differences of approximately 2.5% of the total area while maintaining feasible computation times. We set the N for other regions in proportion to how their area compares to the area of the Central Arctic. Using higher N in general leads to slightly more accurate forecasts, since this difference in area can be modestly reduced. Moderately lowering N in general will have the opposite effect. However, for small adjustments, e.g. adding or removing 5 to 10 lines, this pattern may not hold due to sampling error.

2.5 Prior distribution of the mean sea ice edge

We take a Bayesian approach to parameter estimation. We place a strong prior on $\boldsymbol{\mu}$, the mean sea ice edge, because the ensemble forecast provides considerable information about the likely location of the mean sea ice edge. We first reduce the systematic errors in the ensemble using Contour Shifting Director et al. (2017), a bias-reduction method for ensemble forecasts that we now review.

2.5.1 Contour-Shifting

Director et al. (2017) developed Contour Shifting for the Central Arctic region, and here we extend it to all regions. We summarize the method using the notation in Section 2.

For some historical training period preceding the forecast year, we compare the ice edge predicted by the ensemble mean forecast to the observed ice edge. For each year j and line L_i in a particular region, we record the length of the line segments extending from each point on the coastline, B_i , to the corresponding point on the observed ice edge contour, $\tilde{S}_{i,j}^{obs}$.

We also record the lengths of the line segments from each point on the coastline, B_i , to the corresponding point on the ensemble mean ice edge, $\tilde{S}_{i,j}^{ens}$. We denote these lengths by $\|y_{i,j}^{obs}\|$ and $\|y_{i,j}^{ens}\|$ respectively. Assuming linear change in these lengths over time, we estimate the length to which the sea ice will extend on line L_i at some new time point t for the observed ice edge,

$$\|\hat{y}_{i,t}^{obs}\| = \hat{\alpha}_i^{obs} + \hat{\beta}_i^{obs}t, \quad (11)$$

and the ensemble mean ice edge,

$$\|\hat{y}_{i,t}^{ens}\| = \hat{\alpha}_i^{ens} + \hat{\beta}_i^{ens}t. \quad (12)$$

Here, $\hat{\alpha}_i^{obs}$, $\hat{\alpha}_i^{ens}$, $\hat{\beta}_i^{obs}$, and $\hat{\beta}_i^{ens}$ denote fitted regression coefficients. These regressions are fit using Huber M-estimation, a form of robust linear regression (Huber, 2011).

The difference between $\|\hat{y}_{i,t}^{obs}\|$ and $\|\hat{y}_{i,t}^{ens}\|$ gives the expected difference between the length predicted by the mean ensemble and the length that will be observed at time t . So, the forecasted length on line L_i at time t is expected to be

$$\|\hat{y}_{i,t}^{CS}\| = \|\hat{y}_{i,t}^{ens}\| + (\|\hat{y}_{i,t}^{obs}\| - \|\hat{y}_{i,t}^{ens}\|), \quad (13)$$

where the superscript CS indicates that a Contour Shifting adjustment has been made.

Each adjusted length, $\|\hat{y}_{i,t}^{CS}\|$, can be combined with the corresponding B_i and L_i value as in Section 2.1 to produce new ice edge contours. The resulting contours may have self-intersections at a small number of locations. These self-intersections can be corrected with an iterative application of the Douglas-Peucker algorithm as described in Section 2.1. Contours from ensembles that have been adjusted in this way are referred to as Contour-Shifted and have reduced systematic error compared to initial ensemble forecasts.

2.5.2 Prior for mean proportions ice-covered

We can now incorporate this reduced bias form of the forecasted ensemble mean ice edge contour into the prior for $\boldsymbol{\mu}$. We use the following prior distribution,

$$\boldsymbol{\mu} \sim N(\boldsymbol{\mu}_0, \boldsymbol{\Lambda}_0), \quad (14)$$

where $\boldsymbol{\mu}_0$ is an $n \times 1$ mean vector informed by the ensemble forecast. Let

$$\pi_{i,t}^{CS} = \frac{\|y_{i,t}^{CS} \cap \mathbf{R}_i\|}{\|\mathbf{R}_i\|}. \quad (15)$$

denote the proportion of \mathbf{R}_i that $y_{i,t}^{CS}$ covers in the Contour-Shifted ensemble mean ice edge. Then for all i , let

$$\mu_{0,i} = \begin{cases} \text{logit}(\|\pi_{i,t}^{CS}\|) & \text{for } \epsilon \leq \pi_{i,t}^{CS} \leq 1 - \epsilon \\ \text{logit}(\epsilon) & \text{for } \pi_{i,t}^{CS} < \epsilon \\ \text{logit}(1 - \epsilon) & \text{for } \pi_{i,t}^{CS} > 1 - \epsilon. \end{cases} \quad (16)$$

Also, the matrix $\mathbf{\Lambda}_0$ is a $n \times n$ diagonal covariance matrix with

$$\mathbf{\Lambda}_{0,ii} = \frac{\text{logit}(\max(\pi_{i,t}^{CS} - 0.125, \epsilon)) - \text{logit}(\min(\pi_{i,t}^{CS} + 0.125, 1 - \epsilon))}{\Phi^{-1}(.995)}. \quad (17)$$

This prior covariance treats all μ_i as independent. The variance for each μ_i is equivalent to the variance that would be obtained with 99% of the distribution's mass in the logit-transformed interval of $[\max(\pi_{i,t}^{CS} - 0.125, \epsilon), \min(\pi_{i,t}^{CS} + 0.125, 1 - \epsilon)]$. This prior variance for $\mu_{0,i}$ typically corresponds to the mean proportion being within 0.125 of the Contour-Shifted ensemble mean proportion, $\pi_{i,t}^{CS}$. The variance is reduced if $\pi_{i,t}^{CS}$ is close to 0 or 1. (See Appendix A for the derivation of the standard deviation of a normal distribution that corresponds to a particular proportion of the mass of the distribution being within a set of bounds. In this case, $M = \text{logit}(\max(\pi_{i,t}^{CS} - 0.125, \epsilon))$, $m = \text{logit}(\min(\pi_{i,t}^{CS} + 0.125, 1 - \epsilon))$, and $\gamma = 0.99$.)

2.6 Prior for Covariance

For the prior on $\mathbf{\Sigma}$ we only use information about the physical constraints. While ensembles have the potential to provide information about covariance, the variability of the ensembles we have analyzed do not align with the variability seen in observations. As such, we use only physical constraints to inform our priors for the covariance parameters, σ and κ .

Since standard deviation values are bounded below and considerable differences in variances exist for the $\tilde{\pi}_i$ values, we select an independent uniform prior for each σ_i such that

$$\sigma_{0,i} \stackrel{iid}{\sim} \text{Unif}(\alpha_{\sigma,0}, \beta_{\sigma,0}), \quad (18)$$

where $\alpha_{\sigma,0} = 0.01$. We bound σ at $\alpha_{\sigma,0}$ rather than zero to avoid numerical issues when sampled σ values approach zero. We let

$$\beta_{\sigma,0,i} = \frac{(\text{logit}(\delta_2) - \text{logit}(\delta_1))/2}{\Phi^{-1}(.995)}. \quad (19)$$

where typically $\delta_1 = \epsilon$ and $\delta_2 = 1 - \epsilon$. This upper bound corresponds to the standard deviation of a Gaussian distribution with 99% of the distribution's mass in the interval $(\text{logit}(\delta_1), \text{logit}(\delta_2))$. This prior distribution ensures that the variance of the transformed proportion of ice-covered length does not substantially exceed the variance of a normal

distribution that fully covers the interval of possible proportion values. (This bound is obtained using Appendix A with $M = \text{logit}(\delta_2)$, $m = \text{logit}(\delta_1)$, and $\gamma = 0.99$.)

Exceptions to the typical δ_1 and δ_2 values are made in the Central Arctic region where $\delta_1 = 0.15$ and in the Greenland sea region where $\delta_2 = 0.73$. These exceptions reflect the fact that the ice-covered proportions in these regions have never covered the full interval $[\epsilon, 1 - \epsilon]$ for any L_i in the training observations. Even at the annual minimum, lines in the Central Arctic have never had ice coverage proportions near zero. Similarly, even at the annual maximum, lines in the Greenland sea have never had ice coverage proportions exceeding 0.73.

With little information from which to anticipate how correlation decreases with distance, we use the following vague prior for κ ,

$$\kappa_0 \sim \text{Unif}(\alpha_{\kappa,0}, \beta_{\kappa,0}), \quad (20)$$

where $\alpha_{\kappa,0} = 0.05$ and $\beta_{\kappa,0} = 20$ in our implementation. This prior ensures that κ remains positive.

2.7 Posterior distribution

To fit this model, we need a set of observed contours drawn from the same distribution. We treat the contours in the P years immediately preceding the forecast year as independent samples from the distribution of contours from which the forecast year's contour will be drawn. With this approach we are assuming that the distribution of the contours is stationary over the P -year period. While this stationarity assumption is not strictly true given climate change, for decadal time scales the effects of the climate change trend on sea ice are small relative to year-to-year variability. Therefore, we fix P and assume these recent observations provide a reasonable basis on which to build a Bayesian model. We index the years with the subscripts $j = \{1, 2, \dots, P\}$. We denote the set of n observed proportions in year j by $\tilde{\pi}_j$. The element $\tilde{\pi}_{ij}$ is the proportion of \mathbf{R}_i that y_{ij} covers in year j .

Combining the likelihood for the observed proportions with the prior distributions introduced in Sections 2.5 and 2.6 gives the posterior distribution

$$\prod_{j=1}^P \{p(\tilde{\pi}_j, \boldsymbol{\mu}, \boldsymbol{\sigma}, \kappa)\} p(\boldsymbol{\mu}) p(\boldsymbol{\sigma}) p(\kappa) = \prod_{j=1}^P \{N(\tilde{\pi}_j | \boldsymbol{\mu}, \boldsymbol{\Sigma}(\boldsymbol{\sigma}, \kappa))\} N(\boldsymbol{\mu} | \boldsymbol{\mu}_0, \boldsymbol{\Lambda}_0) \times \prod_{i=1}^n \{\text{Unif}(\sigma_i | \alpha_{\sigma,0}, \beta_{\sigma,0})\} \text{Unif}(\kappa | \alpha_{\kappa,0}, \beta_{\kappa,0}). \quad (21)$$

The posterior means of $\boldsymbol{\mu}$ and $\boldsymbol{\Sigma}$ can be used with Equations 5, 9, and 10 to generate $\tilde{\pi}$.

2.8 Model fitting

We sample from the posterior distribution in Equation 21 for each region independently with Markov chain Monte Carlo (MCMC), using the observed sea ice in the preceding P years. MCMC diagnostics are given in Appendix Section C. Regions that are either completely filled with sea ice or contain no sea ice in all training years are omitted from model fitting. In such cases we predict complete ice-cover or no sea ice respectively. In some months of the year, the observed proportions at the start and/or end of the fixed boundary lines are 0 or 1 for all observed P . We fix these lines with proportions of 0 or 1 rather than fit them. This omission in fitting avoids estimating an excessively high κ due to perfect correlation among the lines in these sections. In the Central Arctic sets of lines bordering the Canadian Archipelago that have proportion 1 for all P years are similarly fixed.

We use Metropolis steps for updating each μ_i , σ_i , and κ . Normal proposals are used for each parameter at each iteration centered at their current value. For each element i and iteration t , the log acceptance ratio for $\mu_i^{(t)}$ is

$$\begin{aligned} & -\frac{1}{2} \sum_{j=1}^P (\tilde{\pi}_j - \boldsymbol{\mu}^{(t)})^T \boldsymbol{\Sigma}^{-1} (\tilde{\pi}_j - \boldsymbol{\mu}^{(t)}) - \frac{1}{2} (\boldsymbol{\mu}^{(t)} - \boldsymbol{\mu}_0)^T \boldsymbol{\Lambda}^{-1} (\boldsymbol{\mu}^{(t)} - \boldsymbol{\mu}_0) \\ & + \frac{1}{2} \sum_{j=1}^P (\tilde{\pi}_j - \boldsymbol{\mu})^T \boldsymbol{\Sigma}^{-1} (\tilde{\pi}_j - \boldsymbol{\mu}) + \frac{1}{2} (\boldsymbol{\mu} - \boldsymbol{\mu}_0)^T \boldsymbol{\Lambda}^{-1} (\boldsymbol{\mu} - \boldsymbol{\mu}_0), \end{aligned} \quad (22)$$

where $\boldsymbol{\mu}^{(t)}$ denotes the $\boldsymbol{\mu}$ vector on the t -th iteration with the i -th element proposed. For each element i and iteration t , the log acceptance ratio for $\sigma_i^{(t)}$ is

$$\begin{aligned} & -\frac{n}{2} \log |(\boldsymbol{\Sigma}^{(t)})| - \frac{1}{2} \sum_{j=1}^P (\tilde{\pi}_j - \boldsymbol{\mu})^T (\boldsymbol{\Sigma}^{(t)})^{-1} (\tilde{\pi}_j - \boldsymbol{\mu}) + \mathbb{1}[\sigma_i^{(t)} \in (\alpha_{\sigma,0}, \beta_{\sigma,0})] \\ & + \frac{n}{2} \log |\boldsymbol{\Sigma}| + \frac{1}{2} \sum_{j=1}^P (\tilde{\pi}_j - \boldsymbol{\mu})^T (\boldsymbol{\Sigma}^{(t)})^{-1} (\tilde{\pi}_j - \boldsymbol{\mu}), \end{aligned} \quad (23)$$

where $\sigma_i^{(t)}$ denotes the proposal for the i -th element of $\boldsymbol{\sigma}$ on the t -iteration and $\boldsymbol{\Sigma}^{(t)}$ denotes the corresponding covariance matrix with $\sigma_i^{(t)}$ proposed. On the t -th iteration, the log acceptance ratio for $\kappa^{(t)}$ is

$$\begin{aligned} & -\frac{n}{2} \log |(\boldsymbol{\Sigma}^{(t)})| - \frac{1}{2} \sum_{j=1}^P (\tilde{\pi}_j - \boldsymbol{\mu})^T (\boldsymbol{\Sigma}^{(t)})^{-1} (\tilde{\pi}_j - \boldsymbol{\mu}) + \mathbb{1}[\kappa^{(t)} \in (\alpha_{\kappa,0}, \beta_{\kappa,0})] \\ & + \frac{n}{2} \log |\boldsymbol{\Sigma}| + \frac{1}{2} \sum_{j=1}^P (\tilde{\pi}_j - \boldsymbol{\mu})^T (\boldsymbol{\Sigma}^{(t)})^{-1} (\tilde{\pi}_j - \boldsymbol{\mu}), \end{aligned} \quad (24)$$

where $\kappa^{(t)}$ denotes the proposal for κ on the t -th iteration and $\boldsymbol{\Sigma}^{(t)}$ now denotes the corresponding covariance matrix with $\kappa^{(t)}$ proposed.

3 Mixture Contour Forecasting

The contour model generally provides reasonable forecasts of the sea ice edge contour, but does have some weaknesses. The first is that these forecasts only focus on the contour. While the vast majority of the sea ice is contained within contiguous areas within the main sea ice edge, small areas of sea ice sometimes still form away from this main area. Areas of open water, called polynyas, also sometimes form as holes within the main sea ice area. The contour model proposed in the previous section cannot represent these features. Secondly, forecasts of this type are tied to the existing ensemble forecast, so if the initial ensemble forecast is not very accurate, such as at long lead times, the resulting forecast will not be very skillful. We address these weaknesses by developing a mixture model that combines the contour model with a climatological forecast that has different strengths and weaknesses.

MCF produces a forecast distribution of ice contours that is a mixture, or weighted average, of two component distributions, the contour model introduced in the previous section and a distribution that represents recent climatology. Here we define the climatology forecast for each grid box as the proportion of times sea ice has been present in that grid box in the P years preceding the forecast year.

The climatology forecast has different advantages and disadvantages. The climatology forecast can represent features such as holes in the sea ice or sea ice away from the main ice edge contours. However, this forecast's reliance on only the small number of observations in the past P years means that it does not capture all plausible ice edge configurations. This weakness of the climatology forecast is greatest in the highly variable months around the sea ice minimum.

The weighting of the two models can be viewed as a simple case of ensemble Bayesian Model Averaging (Raftery et al., 2005). The weight is estimated by maximum likelihood using observations and predictions from preceding years. Let w be the weight of the contour model and $1 - w$ the weight of the climatology distribution. Also, let $\gamma_{s,t}$ be a binary indicator of whether sea ice was present in observations for some grid box s and year t in the training period. Let $g_p(\gamma_{s,t})$ and $g_c(\gamma_{s,t})$ be the estimated Bernoulli probability of sea ice presence in grid box s at time t obtained from the contour model and the climatology respectively. In the former case, the estimated probability is the proportion of the time that grid box s is within the area enclosed by the generated contours for time t . The predicted probability of sea ice presence at grid box s at time t is then

$$p(\gamma_{s,t}) = wg_p(\gamma_{s,t}) + (1 - w)g_c(\gamma_{s,t}) \quad (25)$$

Assuming that errors in space and time are independent, the corresponding log-likelihood

is

$$l(w) = \sum_t \sum_s \log\{w a_s g_p(\gamma_{s,t}) + (1 - w) a_s g_c(\gamma_{s,t})\}. \quad (26)$$

The variable a_s is the proportion of the entire area that is in grid box s , i.e., $\sum_s a_s = 1$. The use of a_s accounts for the fact that the grid boxes do not all have the same area. Assuming spatial and temporal independence is almost certainly inaccurate; however, Raftery et al. (2005) found in a similar case that results were not particularly sensitive to this assumption.

To maximize this log-likelihood we use the Expectation-Maximization algorithm (Dempster et al., 1977). This optimization algorithm can be applied in situations where if some unobserved quantity were known, estimation of the variable(s) of interest would be simple. In this case estimating w would be straightforward if we knew for every grid box and time point whether the climatology model or the contour model estimated the observed sea ice presence more accurately. So, we introduce the latent variable $z_{p,s,t}$, which has value 1 if the contour model is the best forecast for grid box s in year t and 0 otherwise. The variable $z_{c,s,t}$ is defined analogously for climatology. Note that only one of the parameters $z_{c,s,t}$ or $z_{p,s,t}$ could truly be 1; but for estimation these parameters can take any value in the interval $[0, 1]$. Also, note $\hat{z}_{p,s,t} = 1 - \hat{z}_{c,s,t}$. Then the E-step is

$$\hat{z}_{p,s,t}^{(j)} = \frac{w^{(j-1)} a_s g_p(\gamma_{s,t})}{w^{(j-1)} a_s g_p(\gamma_{s,t}) + (1 - w^{(j-1)}) a_s g_c(\gamma_{s,t})}, \quad (27)$$

and the M-step is

$$w^{(j)} = \frac{\sum_t \sum_s a_s \hat{z}_{p,s,t}^{(j)}}{\sum_t \sum_s a_s} \quad (28)$$

for the j -th iteration. To avoid degeneracies, any (s, t) pairs where $g_p(\gamma_{s,t}) = g_c(\gamma_{s,t})$ are omitted from this maximization. Therefore, the denominator in Equation 28 may be unequal to the number of years in the training period.

4 Method evaluation

4.1 Model outputs and observations

All post-processing methods are applied to the fifth generation of the European Centre for Medium-Range Weather Forecasts (ECMWF) seasonal forecasting system (SEAS5) (Johnson et al., 2019; European Centre for Medium-Range Weather Forecasts, 2017). The relevant sea ice concentration model output can be downloaded from the Copernicus Climate Change

Service Climate Data Store (Copernicus Climate Change Service, 2019). Among a set of publicly available ensembles without post-processing, ECMWF has been shown to be generally the most skillful (Zampieri et al., 2018). The 25-member ensemble ECMWF forecasts are initialized monthly and extend to 215 days. Model output was regridded to the National Snow and Ice Data Center Polar stereographic grid with an approximately 25km by 25km grid (National Snow and Ice Data Center, 2017) using a nearest-neighbors method (Zhuang, 2018). Daily model output was averaged to monthly to match observations.

We evaluate forecast accuracy by comparing predictions to a monthly-averaged sea ice concentration produced from the National Aeronautics and Space Administration satellites Nimbus-7 SMMR and DMSP SSM/I-SSMIS. This data can be downloaded from the National Snow and Ice Data Center (Comiso, 2017). Grid boxes with sea ice concentrations of at least 15% are treated as having sea ice present. Otherwise grid boxes are treated as not containing sea ice.

We evaluate forecasting skill for monthly-averaged sea ice at lead times of 0.5 months to 6.5 months in the year 2008-2016. We report lead times treating the monthly mean as the halfway point within a month. For example, the 0.5-month lead forecast for January refers to the average of the first 31 days of a forecast initialized on January 1st. Grid boxes that are coded as land in the observations, the ensemble, or the *IceCast* R package (Director et al., 2020) are treated as land.

The forecasts previously described are summarized in lines 1-4 of Table 1. Beginning in 1993, all years preceding the forecast year are used in fitting Contour Shifting. A ten-year rolling window is used to fit the statistical model for generating contours and in the climatology forecast weighted in MCF. The time length of ten years is used, since recent analyses have shown that climatology computed over a ten-year period provides reasonably accurate sea ice forecasts. Such forecasts become nearly as accurate as ECMWF ensemble forecasts at lead times of 1.5 months (Zampieri et al., 2018). Slight changes in the number of years used for this purpose is unlikely to affect the results. However, using many fewer years would not provide enough samples to fit the parameters accurately. Using a much bigger number of years would also degrade performance. Because of the rapid reduction in Arctic sea ice area, contours from past decades will differ notably from recent ice edge contours. A three-year rolling window is used to determine the weights in MCF. Performance accuracy is generally insensitive to this choice (see Appendix D). One hundred contours are generated for each forecast.

Table 1: Summary of forecast types evaluated. Probabilistic forecasts give estimates in the interval $[0, 1]$ and binary forecasts indicate predicted sea ice presence

Forecast	Probabilistic	Binary
Ensemble	proportion of ensemble members predicting sea ice	indicator of whether median ensemble member predicts sea ice
Contour	ensemble mean forecast bias-corrected with Contour-Shifting and calibrated by generating contours	ensemble mean forecast adjusted with Contour-Shifting
Climatology	proportion of observations in the 10 years preceding the forecast year that contain sea ice	indicator of whether at least five of the ten years preceding the forecast year contained sea ice
Mixture Contour Forecast (MCF)	forecast formed by weighting probability densities from climatology and the contour model	indicator of whether forecast formed by weighting probability densities from climatology and the contour model predicts sea ice with $p \geq 0.5$
Trend Adjusted Quantile Mapping (TAQM)	ensemble post-processed using technique in Dirkson et al. (2019b)	NA
Damped Persistence	NA	indicator of whether predicted sea ice concentration from a damped persistence forecast is at least 0.15 (modified from Wayand et al. (2019))

4.2 Reference forecasts

We compare our results to two additional reference forecasts summarized in lines 5-6 of Table 1. Trend Adjusted Quantile Mapping (TAQM) is another recently developed statistical post-processing method for sea ice (Dirkson et al., 2019b). TAQM fits a parametric probability distribution to ensemble model output and applies a specialized version of quantile mapping to produce probabilistic forecasts of sea ice concentration. TAQM does not predict the probability of sea ice presence directly, but Dirkson et al. (2019b) do use the resulting distribution of the sea ice concentration to predict the probability of sea ice presence (concentration of at least 15%).

We also compute a damped persistence forecast in a manner similar to Wayand et al. (2019). Damped persistence forecasts estimate the sea ice concentration in forecast month

m using linear regression and the observed sea ice concentration in the initialization month i . For each grid box, the concentration for month m in year t , denoted by $C_{m,t}$, is estimated as

$$\hat{C}_{m,t} = \hat{\beta}_m t + (C_{i,t_i} - \hat{\beta}_i t_i) \hat{\rho}, \quad (29)$$

where C_{i,t_i} is the observed concentration in the i -th initialization month, $\hat{\beta}_m$ and $\hat{\beta}_i$ are the coefficients for linear regressions of C_m and C_i on year, and $\hat{\rho}$ is the empirical correlation of C_m and C_i estimated from past observations. If all values of C_m and/or C_i in the training period are the same, the empirical correlation is undefined. In these cases, we set $\hat{\rho}$ to 0, which makes Equation 29 equivalent to linear regression. When $i \leq m$, $t_i = t$, otherwise $t_i = t - 1$. Grid boxes with predicted concentration of at least 0.15 are forecasted to contain sea ice. Observations beginning in 1981 and extending up to the initialization time are used in fitting.

4.3 Visualizing forecasts

Uncertainty information is needed for maritime planning to adequately evaluate risks and benefits. Like Gneiting et al. (2007), we consider accurate model calibration to be vital for probabilistic forecasts. We illustrate the importance of calibration in this context with Figure 5, which shows samples of four probabilistic forecasts for September 2008. The corresponding observed sea ice edge for September 2008 is also plotted for reference. Figure 5 illustrates the types of forecasting errors that can occur when forecasts are not calibrated. Specifically, events with low predicted probability occur more often than expected, and/or events with high predicted probability occur less often than expected.

For the contour model and MCF, the observed contour is almost entirely contained within regions with positive probability and has only small areas where sea ice is predicted with probability 1 but sea ice is not present in observations. The MCF forecast is slightly more variable than the contour model, reflecting its weighting with climatology. Since w is high for September at a 1.5-month lead time, the difference between the contour model and MCF is small. In cases where w , the weight on the contour model, is lower, the difference between the contour model and MCF may be more substantial. For the climatology and ensemble forecasts, the observed contour goes through some regions with zero probability, suggesting that these forecasts are not sufficiently variable. For these forecasts, there are areas where sea ice is predicted with probability 0, but sea ice is observed. Discrepancies like these between the forecasted probability and what will likely occur makes maritime planning and risk mitigation with these latter types of forecasts difficult.

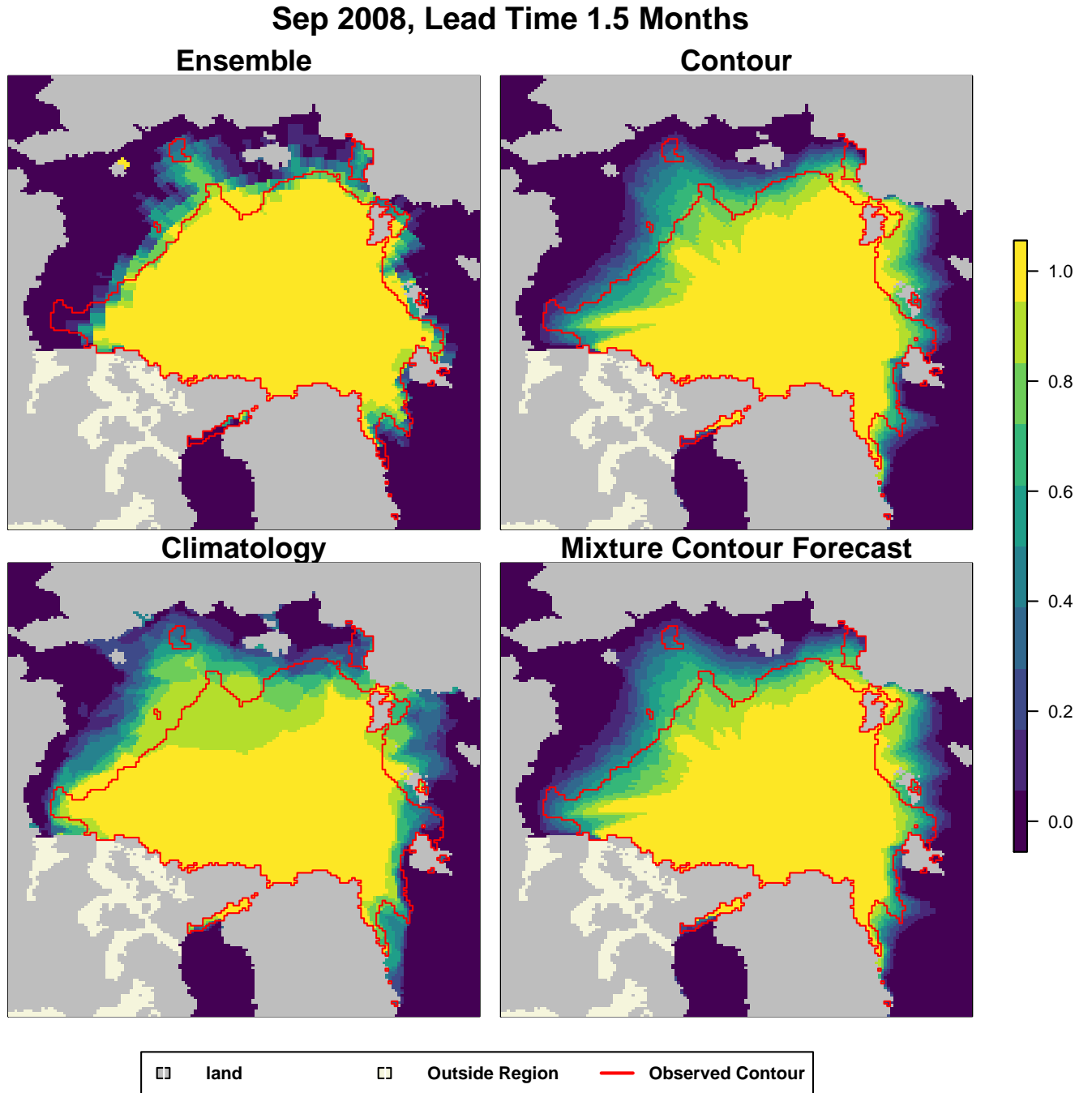


Figure 5: Forecasts of the probability of sea ice presence for September 2008 using different methods. The forecasts are described in Table 1. The red line is the observed sea ice edge contour and grey areas are land. For MCF, the observed ice edge is almost completely within areas with positive probability and has little area where sea ice was predicted with probability 1 but sea ice was not present in observations. In contrast, the observed sea ice edge more often goes through regions with zero probability in the ensemble and climatology forecasts. In the climatology forecast, there is also the most area where sea ice is predicted with probability 1 but is not present in observations.

4.4 Assessing Calibration

We now evaluate model calibration for the probabilistic forecasts. We evaluate calibration with reliability diagrams that plot the forecasted probability of observing sea ice against the proportion of times sea ice was observed. A perfectly calibrated forecast would have all points on the $y = x$ line, i.e. grid boxes forecasted to contain sea ice with a given probability actually contain sea ice the same proportion of the time. So, the closer the points lie to the $y = x$ line, the better calibrated the forecast is.

Shipping varies seasonally in the Arctic, with more shipping in months around the annual sea ice minimum in September (Ellis and Brigham, 2009), so we emphasize performance in these peak shipping months. In Figure 6 we show the reliability diagrams for the peak-shipping months for the probabilistic forecasts. Predictions from MCF are substantially better calibrated than the ensemble and better calibrated than TAQM during these months, especially at short lead times. Figures 12 and 13 in Appendix B show that MCF always improves calibration over the unadjusted ensemble and generally improves calibration compared to TAQM. We note that MCF has been designed specifically for predicting sea ice presence, while TAQM addresses the more general goal of forecasting sea ice concentration. The difference in calibration performance between MCF and TAQM highlights the benefit for maritime planning of having a method focused exclusively on predicting sea ice presence. TAQM remains valuable for its broader applicability.

4.5 Assessing accuracy

We evaluate forecast accuracy using Brier scores (Brier, 1950). We compute average area-weighted Brier scores over the $T = 9$ years in the test set as

$$\frac{\sum_t \sum_s a_s (f_{s,t} - o_{s,t})^2}{T}, \quad (30)$$

where $f_{s,t}$ and $o_{s,t}$ denote the forecast and observation in grid box s in year t respectively. The value a_s is the proportion of the total area that is in grid box s . The observed value is 1 when the sea ice concentration is at least 0.15, and 0 otherwise. For probabilistic forecasts, $f_{i,j} \in [0, 1]$ and for binary forecasts, $f_{i,j} \in \{0, 1\}$.

In Figure 7, we plot the average Brier score in peak-shipping months by lead time for the probabilistic forecasts. The ensemble forecasts typically have increasing Brier scores as lead time increases. Our contour model generally improves forecast accuracy and MCF improves accuracy further. As lead time increases, MCF’s performance converges to equal or better performance than climatology. TAQM also generally improves accuracy of forecasts.

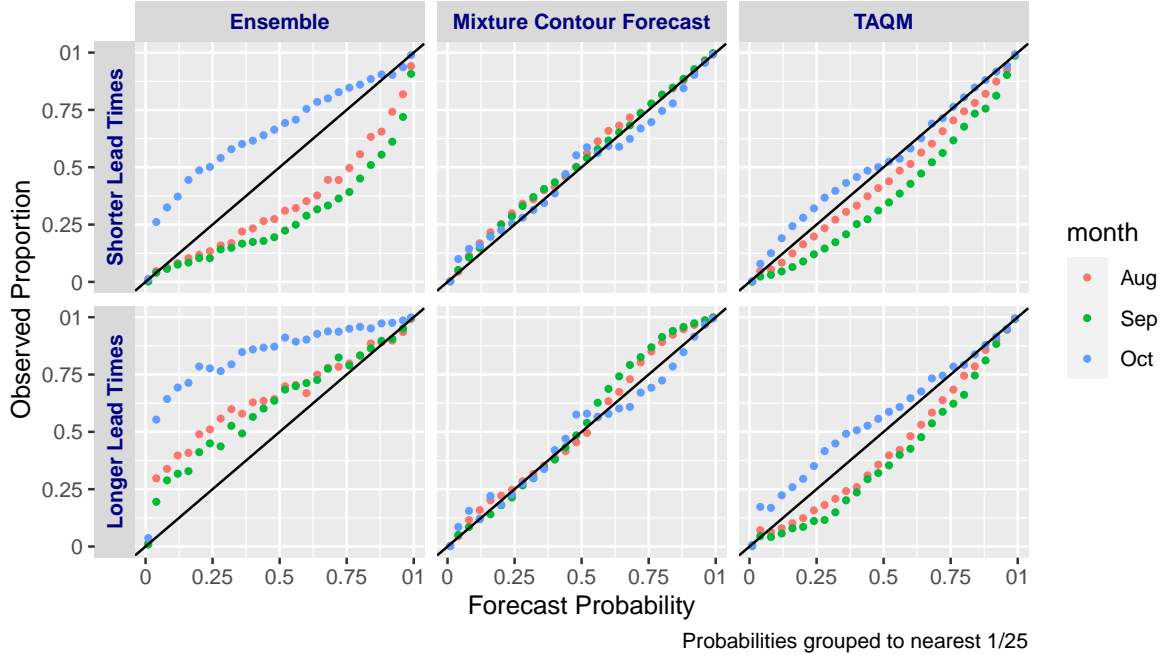


Figure 6: The average proportion of the time sea ice was present plotted against the predicted probability of sea ice presence for the raw ECMWF forecasts (left), after post-processing with MCF (middle), and TAQM (right). Forecasts are grouped into lead times of 0.5 and 1.5 months (top) and 2.5-6.5 months (bottom). A perfectly calibrated forecast would have all points on the diagonal $y = x$ line.

Figures ?? and 10 in Appendix B show that TAQM and MCF have similar overall accuracy, but that the pattern of their performance by lead time and month varies. For peak shipping months, MCF outperforms TAQM, suggesting that our specialized modeling of the sea ice edge has benefits for maritime planning use. For other applications, more general techniques like TAQM may be more appropriate. For the shortest lead time of 0.5 months, the damped persistence forecast performs best, but its skill decays rapidly with lead time. The performance of the damped persistence forecast indicates that there could be a role for the current observed state of the sea ice in forecasting, but that the role would need to be restricted to very short lead times. In summary, MCF provides the best calibrated forecasts year round and accurate forecasts during peak-shipping months.

4.6 Binary Forecasts

We also briefly assess binary forecasts with the bottom panel in Figure 7. Binary forecasts are inherently poorly calibrated, and so are not optimal, but can be useful in method assessment. The Contour-Shifted forecast clearly improves accuracy compared to the ensemble. In other words, Contour Shifting does reduce some systematic bias that affects typical en-

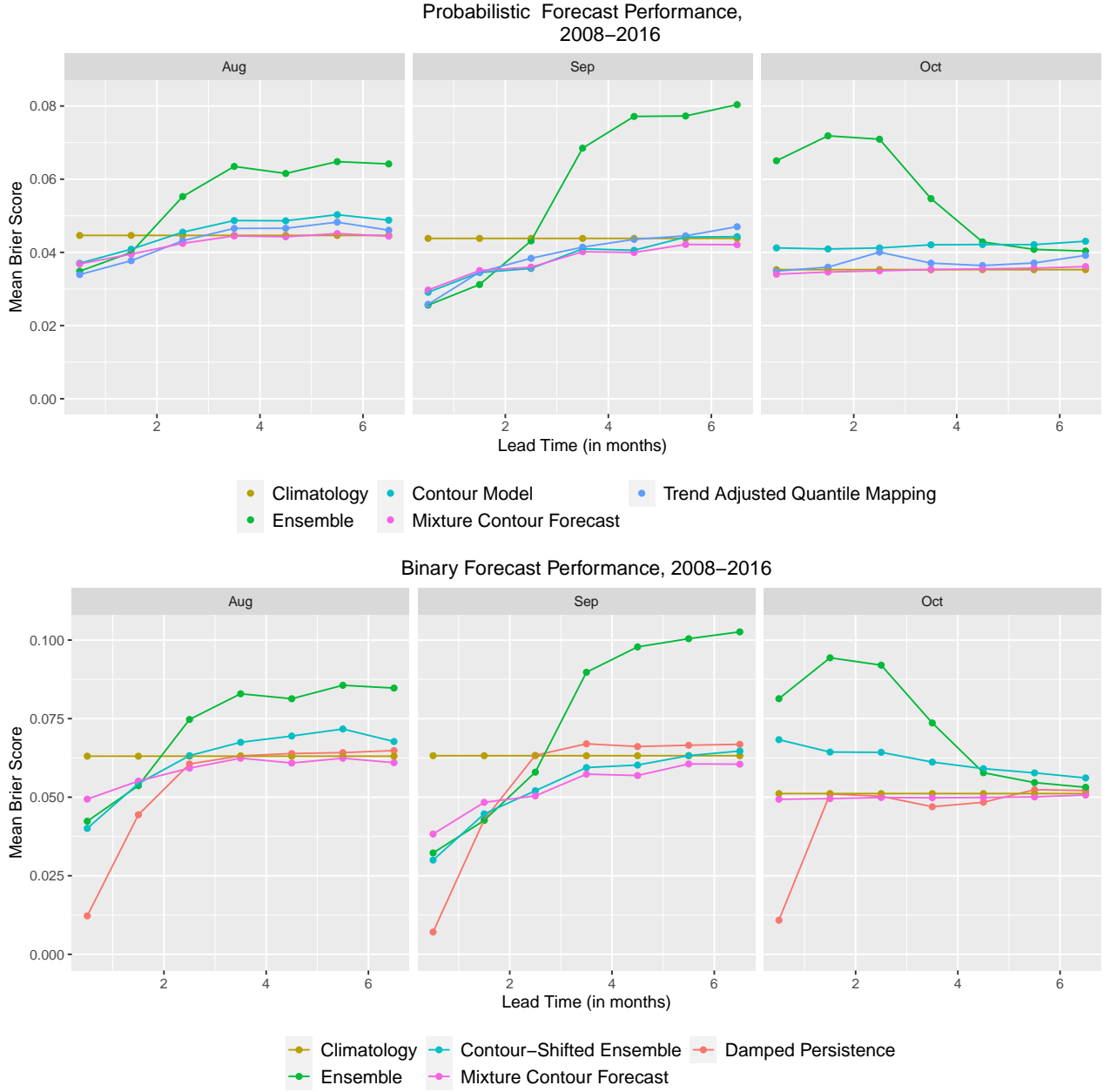


Figure 7: Top: Average Brier scores by month for the test years 2008-2016 for the probabilistic forecasts. The Brier Score for each grid box is weighted based on its area. Forecasts are described in Table 1. Bottom: As above, but for the binary forecasts.

sembles. Binary MCF performs similarly to the Contour-Shifted ensemble in general, but MCF substantially outperforms the Contour-Shifted ensemble when the ensemble forecast is poor. This case illustrates that the adaptive weighting provided by MCF is valuable when issuing binary forecasts as well as probabilistic forecasts. Brier scores for binary forecasts for all seasons are in 11 in Appendix B.

4.7 Understanding mixture weights

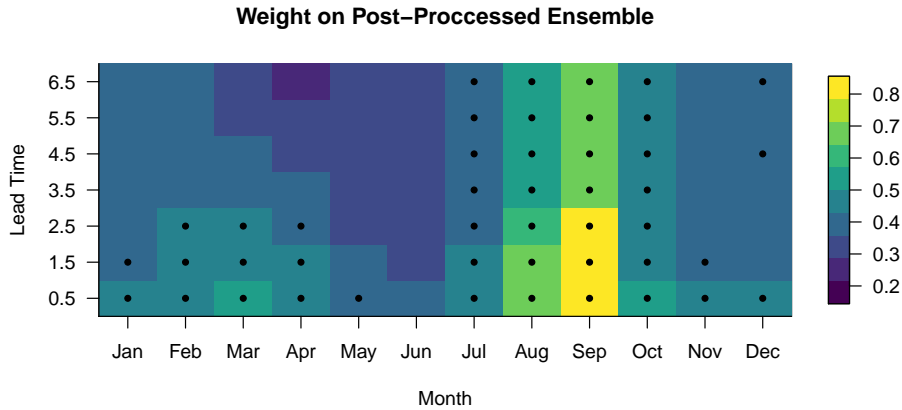


Figure 8: Weight on the contour model by month and lead time. A black dot indicates that the weight is at least 0.4. The contour gets more weight at short lead times and in months near the sea ice minimum. The weight on climatology is equal to one minus the weight on the contour model.

Since MCF is fitted separately for each forecast month and lead time, we can examine how the weights on the contour model and climatology forecast vary between months and lead times. Figure 8 shows the average weight placed on the contour model for the years in the test set. High weights typically occur at short lead times, reflecting the fact that the ensemble typically has the most skill soon after it is initialized. High weights also occur in months around the sea ice minimum in September. These are periods of high year-to-year variability, so climatology tends to perform poorly and the ensemble’s ability to simulate evolving physical conditions becomes more important.

5 Discussion

We have introduced the Mixture Contour Forecasting method for issuing probabilistic sea ice forecasts. MCF forecasts are probabilistic and well calibrated, meaning that their predicted

probability of sea ice presence at a given location approximately matches the proportion of times sea ice will be observed at these locations. At most lead times and forecast months, probabilistic MCF forecasts are also as or more accurate than the raw ECMWF ensemble and the other post-processed and statistical forecasts.

Because MCF provides well calibrated and relatively accurate forecasts, MCF’s use has the potential to increase operational sea ice forecasting skill and thereby improve maritime planning in the Arctic. As Arctic routes are planned, the risk of encountering sea ice where it is not expected must be weighed against the cost savings of a shorter route. Vessels in the Arctic have an ice classification that says where they can legally and safely travel. For vessels that are easily damaged in sea ice, encountering any sea ice poses great risk. In contrast, ships that are designed to travel safely through sea ice may gain speed and efficiency by avoiding sea ice, but do not face danger if they encounter it.

Our model evaluation weights both types of misclassification errors equally (predicting the presence of sea ice when it was not observed and predicting the absence of sea ice when it was observed.) However, the probabilistic forecasts provided by MCF do allow us to account for different costs of the two types of error. In particular, MCF opens up the possibility of planning routes using decisions rules that incorporate the probability of sea ice presence. For example, a ship that has high risk of damage when traversing sea ice might elect to only consider routes through areas with very low probability of sea ice.

We have also developed a framework for directly modeling contours. While forecasts could likely be made with field-based geostatistical models (e.g., Zimmerman and Stein, 2010) or by identifying the exceedance level contours estimated from fields (Bolin and Lindgren, 2015; French and Hoeting, 2016), these approaches may have limitations for this application. Most of the error in sea ice forecasts occurs in the region where a rapid transition from fully ice-covered regions to open water occurs (Tietsche et al., 2014). Whether sea ice will be found in grid boxes in the interior of the sea ice region and far from the sea ice edge is essentially known in advance. So placing the majority of the computational cost and modeling effort on the boundary is advantageous. MCF provides a framework for modeling that could be extended to other situations where the boundary is of interest.

As implemented in this paper, estimates of the covariance of the sea ice edge are based on the covariance estimated from the preceding years. These estimates are therefore independent of the covariance of the sea ice edge in the ensemble members. However, the ensemble could plausibly give information about the expected covariance that could not be obtained from past observations. For example, sea ice is expected to continue to become thinner. Thinner sea ice is more affected by variation in meteorological conditions, so the variance of sea ice extent will likely increase (Holland et al., 2011). Effects like these are captured

by the ensemble, but are not in past observations. As such, incorporating the covariance in the ensemble could further improve forecast skill. However, the spread of the ensemble does align with observed variability and the relationship between variability in observations and variability in the ensemble is inconsistent both spatially and temporally. Thus assessment of when the ensemble covariance is informative and how it relates to the observed covariance is needed before it will be feasible to incorporate the ensemble covariance into MCF.

The ECMWF ensemble used in Section 4 is not the only ensemble prediction system. The post-processing techniques developed in this paper could be directly applied to other ensembles, since they do not use any specific features of the ECMWF ensemble. However, model biases and calibration issues vary, so exact performance would need to be assessed. Different ensembles also vary by which forecast months they perform well in, and vary more by the extent to which skill declines with lead time (Zampieri et al., 2018). Thus extending MCF to use multiple ensemble members as has been done for other meteorological variables could provide further skill (e.g., Raftery et al., 2005; Dirkson et al., 2019a).

Our analysis of sea ice forecasting highlights situations where statistical post-processing can provide value. Many aspects of physical processes are known to evolve following well established equations. Such information can only be crudely approximated with a purely observational data-driven approach. On the other hand, physical models are often biased or poorly calibrated, and statistical post-processing methods can be effective in remedying these problems. Combining the strengths of physical and statistical modeling can create predictions that are more accurate than either modeling framework alone.

References

- Blanchard-Wrigglesworth, E., Cullather, R. I., Wang, W., Zhang, J., and Bitz, C. M. (2015). Model forecast skill and sensitivity to initial conditions in the seasonal Sea Ice Outlook. *Geophysical Research Letters*, 42(19):8042–8048.
- Bolin, D. and Lindgren, F. (2015). Excursion and contour uncertainty regions for latent gaussian models. *Journal of the Royal Statistical Society: Series B (Statistical Methodology)*, 77(1):85–106.
- Brier, G. (1950). Verification of forecasts expressed in terms of probability. *Monthly Weather Review*, 78(1):1–3.
- Bushuk, M., Msadek, R., Winton, M., Vecchi, G. A., Gudgel, R., Rosati, A., and Yang, X. (2017). Skillful regional prediction of Arctic sea ice on seasonal timescales. *Geophysical Research Letters*, 44(10):4953–4964.
- Cavalieri, D. J. and Parkinson, C. L. (2012). Arctic sea ice variability and trends, 1979-2010. *The Cryosphere*, 6(4):881.
- Chevallier, M., Salas y Mélia, D., Voldoire, A., Déqué, M., and Garric, G. (2013). Seasonal forecasts of the pan-Arctic sea ice extent using a GCM-based seasonal prediction system. *Journal of Climate*, 26(16):6092–6104.
- Comiso, J. (2017). Bootstrap sea ice concentrations from Nimbus-7 SMMR and DMSP SSM/I-SSMIS. version 3.
- Comiso, J. C., Parkinson, C. L., Gersten, R., and Stock, L. (2008). Accelerated decline in the Arctic sea ice cover. *Geophysical Research Letters*, 35(1).
- Copernicus Climate Change Service (2019). Copernicus climate change service climate data store. <https://cds.climate.copernicus.eu>.
- Dempster, A. P., Laird, N. M., and Rubin, D. B. (1977). Maximum likelihood from incomplete data via the EM algorithm. *Journal of the Royal Statistical Society: Series B (Methodological)*, 39(1):1–22.
- Director, H. M., Raftery, A. E., and Bitz, C. M. (2017). Improved sea ice forecasting through spatiotemporal bias correction. *Journal of Climate*, 30(23):9493–9510.

- Director, H. M., Raftery, A. E., and Bitz, C. M. (2020). Icecast: Apply statistical post-processing to improve sea ice predictions. R package version 3.0.0, <https://github.com/hdirector/IceCastV3>.
- Dirkson, A., Denis, B., and Merryfield, W. J. (2019a). A multimodel approach for improving seasonal probabilistic forecasts of regional arctic sea ice. *Geophysical Research Letters*.
- Dirkson, A., Merryfield, W. J., and Monahan, A. H. (2019b). Calibrated probabilistic forecasts of Arctic sea ice concentration. *Journal of Climate*, 32(4):1251–1271.
- Douglas, D. H. and Peucker, T. K. (1973). Algorithms for the reduction of the number of points required to represent a digitized line or its caricature. *Cartographica: the international journal for geographic information and geovisualization*, 10(2):112–122.
- Ellis, B. and Brigham, L. (2009). Arctic marine shipping assessment 2009 report.
- European Centre for Medium-Range Weather Forecasts (2017). ECMWF SEAS5 user guide. https://www.ecmwf.int/sites/default/files/medialibrary/2017-10/System5_guide.pdf.
- French, J. P. and Hoeting, J. A. (2016). Credible regions for exceedance sets of geostatistical data. *Environmetrics*, 27(1):4–14.
- Gneiting, T. (2013). Strictly and non-strictly positive definite functions on spheres. *Bernoulli*, 19(4):1327–1349.
- Gneiting, T., Balabdaoui, F., and Raftery, A. E. (2007). Probabilistic forecasts, calibration and sharpness. *Journal of the Royal Statistical Society: Series B (Statistical Methodology)*, 69(2):243–268.
- Guemas, V., Blanchard-Wrigglesworth, E., Chevallier, M., Day, J. J., Déqué, M., Doblas-Reyes, F. J., Fučkar, N. S., Germe, A., Hawkins, E., Keeley, S., et al. (2016). A review on Arctic sea-ice predictability and prediction on seasonal to decadal time-scales. *Quarterly Journal of the Royal Meteorological Society*, 142(695):546–561.
- Holland, M. M., Bailey, D. A., and Vavrus, S. (2011). Inherent sea ice predictability in the rapidly changing Arctic environment of the Community Climate System Model, version 3. *Climate Dynamics*, 36(7-8):1239–1253.
- Huber, P. J. (2011). *Robust Statistics*. Springer.

- Johnson, S. J., Stockdale, T. N., Ferranti, L., Balmaseda, M. A., Molteni, F. and Magnusson, L., Tietsche, S., Decremet, D., Weisheimer, A., Balsamo, G., Keeley, S. P. E., Mogensen, K., Zuo, H., and Monge-Sanz, B. M. (2019). SEAS5: the new ECMWF seasonal forecast system. *Geoscientific Model Development*, 12(3).
- Melia, N., Haines, K., and Hawkins, E. (2016). Sea ice decline and 21st century trans-Arctic shipping routes. *Geophysical Research Letters*, 43(18):9720–9728.
- Msadek, R., Vecchi, G. A., Winton, M., and Gudgel, R. G. (2014). Importance of initial conditions in seasonal predictions of Arctic sea ice extent. *Geophysical Research Letters*, 41(14):5208–5215.
- National Snow and Ice Data Center (2017). Region mask for the Northern Hemisphere. http://nsidc.org/data/polar-stereo/tools_masks.html.
- Plummer, M., Best, N., Cowles, K., and Vines, K. (2006). Coda: Convergence diagnosis and output analysis for mcmc. *R News*, 6(1):7–11.
- Raftery, A. E., Gneiting, T., Balabdaoui, F., and Polakowski, M. (2005). Using Bayesian model averaging to calibrate forecast ensembles. *Monthly Weather Review*, 133(5):1155–1174.
- Raftery, A. E. and Lewis, S. M. (1992). Practical Markov chain Monte Carlo: comment: one long run with diagnostics: implementation strategies for Markov chain Monte Carlo. *Statistical Science*, 7(4):493–497.
- Raftery, A. E. and Lewis, S. M. (1995). The number of iterations, convergence diagnostics and generic metropolis algorithms. *Practical Markov Chain Monte Carlo*, 7(98):763–773.
- Sigmond, M., Fyfe, J. C., Flato, G. M., Kharin, V. V., and Merryfield, W. J. (2013). Seasonal forecast skill of Arctic sea ice area in a dynamical forecast system. *Geophysical Research Letters*, 40(3):529–534.
- Smith, L. C. and Stephenson, S. R. (2013). New Trans-Arctic shipping routes navigable by midcentury. *Proceedings of the National Academy of Sciences*, 110(13):E1191–E1195.
- Stroeve, J. C., Serreze, M. C., Holland, M. M., Kay, J. E., Malanik, J., and Barrett, A. P. (2012). The Arctic’s rapidly shrinking sea ice cover: a research synthesis. *Climatic Change*, 110(3-4):1005–1027.

- Tietsche, S., Day, J. J., Guemas, V., Hurlin, W. J., Keeley, S. P. E., Matei, D., Msadek, R., Collins, M., and Hawkins, E. (2014). Seasonal to interannual Arctic sea ice predictability in current global climate models. *Geophysical Research Letters*, 41(3):1035–1043.
- Wang, W., Chen, M., and Kumar, A. (2013). Seasonal prediction of Arctic sea ice extent from a coupled dynamical forecast system. *Monthly Weather Review*, 141(4):1375–1394.
- Wayand, N. E., Bitz, C. M., and Blanchard-Wrigglesworth, E. (2019). A year-round subseasonal-to-seasonal sea ice prediction portal. *Geophysical Research Letters*, 46(6):3298–3307.
- Zampieri, L., Goessling, H. F., and Jung, T. (2018). Bright prospects for Arctic sea ice prediction on subseasonal time scales. *Geophysical Research Letters*, 45(18):9731–9738.
- Zhang, B. and Cressie, N. (2019). Estimating spatial changes over time of Arctic Sea ice using hidden 2×2 tables. *Journal of Time Series Analysis*, 40(3):288–311.
- Zhang, B. and Cressie, N. (2020). Bayesian inference of spatio-temporal changes of Arctic sea ice. *Bayesian Analysis*, 15(2):605–631.
- Zhuang, J. (2018). xesmf: Universal regridding for geospatial data.
- Zimmerman, D. L. and Stein, M. L. (2010). Classical geostatistical methods. In Gelfand, A. E., Diggle, P., Guttorp, P., and Fuentes, M., editors, *Handbook of Spatial Statistics*, pages 29–44. CRC Press: Boca Raton, FL.

Appendices

A Standard deviation corresponding to γ proportion of mass of a Gaussian within symmetric bounds

Consider a Gaussian distribution with known mean $\mu = (m + M)/2$, where $M > m$. The standard deviation, $\sigma > 0$, such that $100 \times \gamma$ percent of the mass of the distribution is within m and M is

$$\sigma = \frac{(M - m)/2}{\Phi^{-1}((1 + \gamma)/2)} \quad (31)$$

where $\gamma \in (0, 1)$ and $\Phi^{-1}(\cdot)$ is the standard normal inverse cumulative distribution function.

Proof. Let X be a random variable with $X \sim N(\mu, \sigma)$. Note that the value of σ that produces $\Pr(m \leq X \leq M) = \gamma$ is equivalent to the value of σ that produces $\Pr(x \leq M) = (1 - \gamma)/2 + \gamma = (1 + \gamma)/2$. Then,

$$\Pr\left(Z \leq \frac{M - (M + m)/2}{\sigma}\right) = \Pr\left(Z \leq \frac{(M - m)/2}{\sigma}\right) = \frac{(1 + \gamma)}{2}$$

Hence,

$$\frac{(M - m)/2}{\sigma} = \Phi^{-1}\left(\frac{1 + \gamma}{2}\right). \quad (32)$$

□

B Additional figures

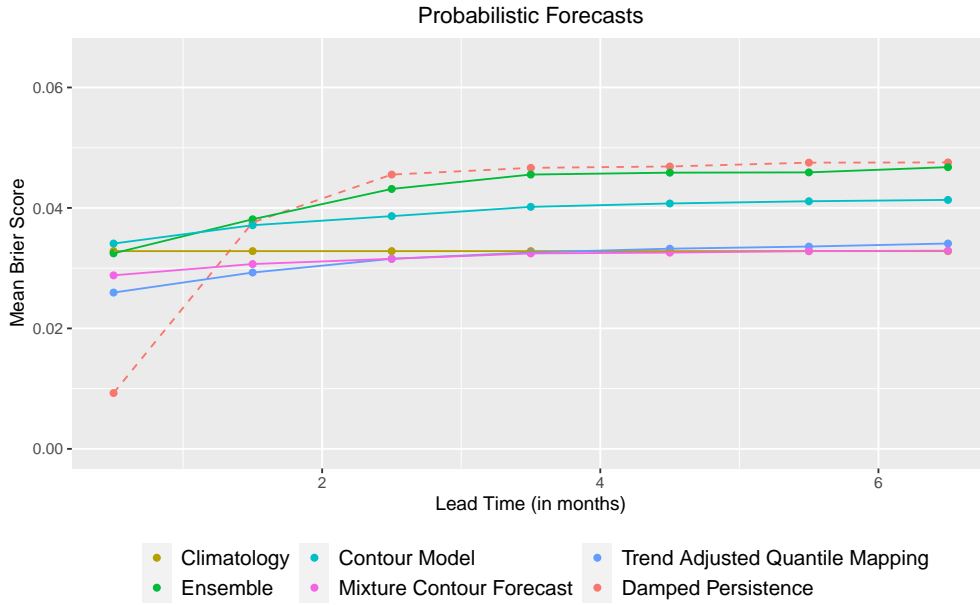


Figure 9: Overall Brier scores for the test years 2008-2016 for the probabilistic forecasts and a damped persistence reference binary forecast. The Brier Score for each grid box is weighted based on its area. Forecasts are described in Table 1 in the main text.

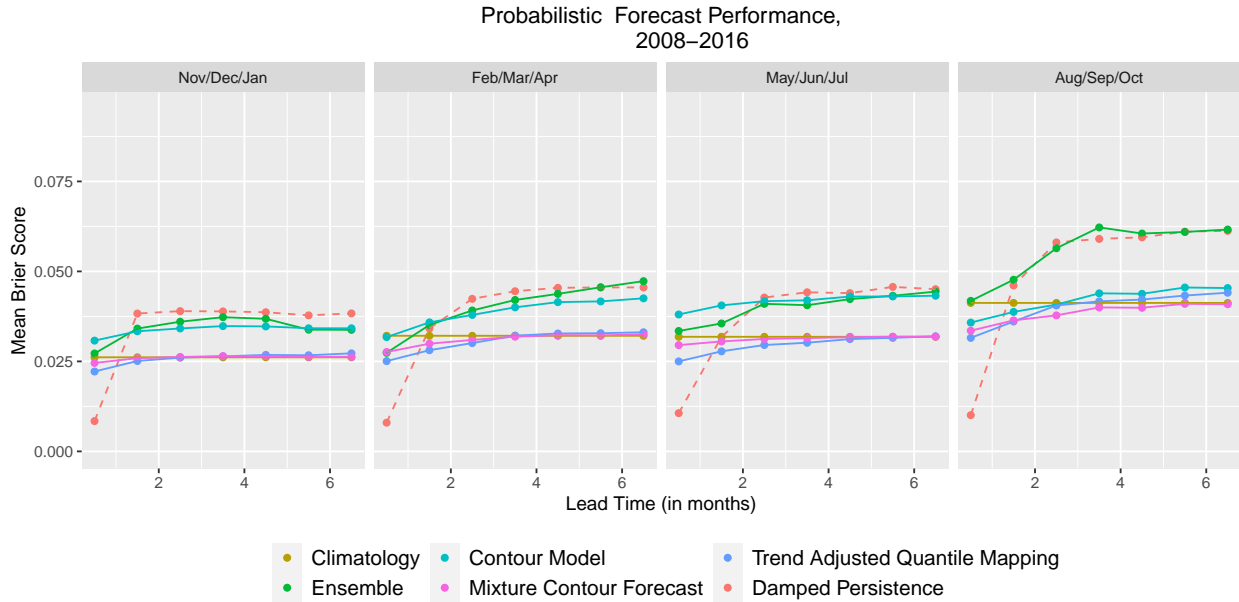


Figure 10: Average Brier scores grouped into three-month sets for the test years 2008-2016 for the probabilistic forecasts and a damped persistence reference binary forecast. The Brier Score for each grid box is weighted based on its area. Forecasts are described in Table 1 in the main text.

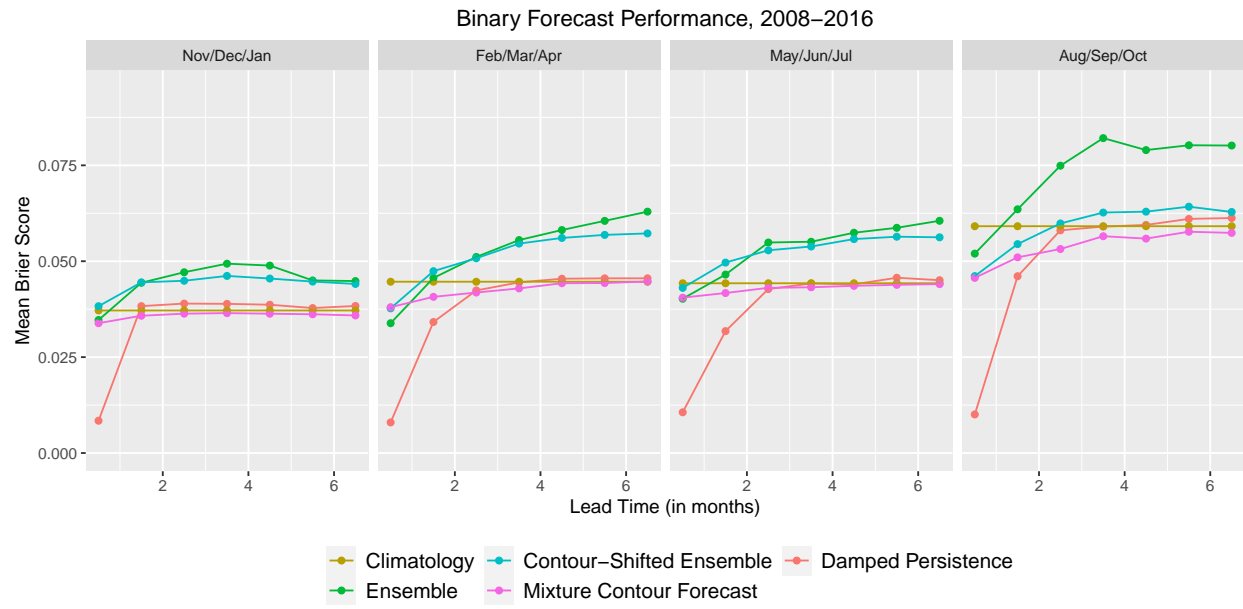


Figure 11: As in Figure 10, except for binary forecasts.

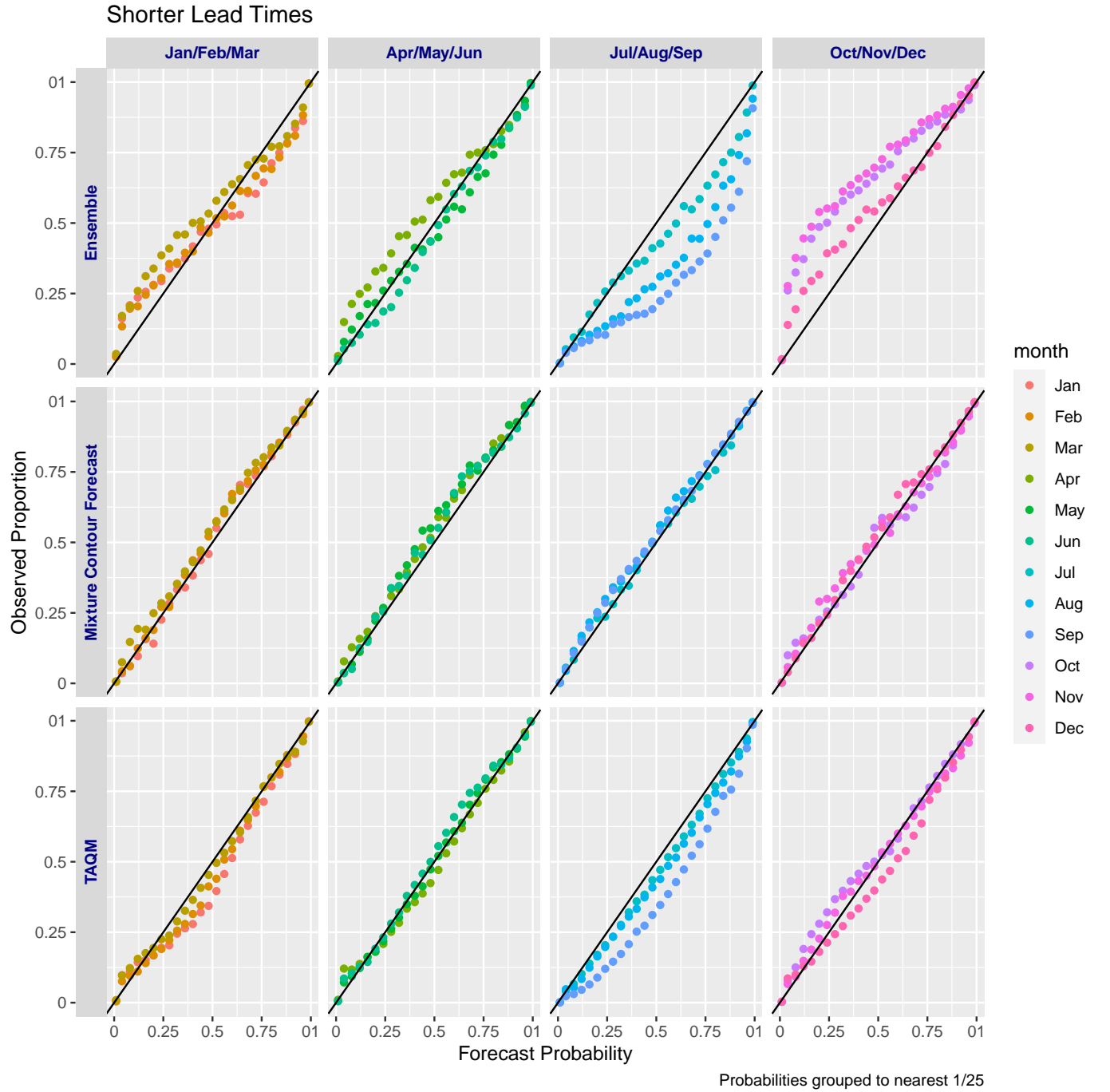


Figure 12: Plots of the average proportion of times sea ice was present against the predicted probability of sea ice presence for the raw ECMWF (top), MCF (middle), and TAQM (bottom) forecasts for lead times of 0.5 - 1.5 months. Results are grouped into three-month sets and all grid boxes are equally weighted.

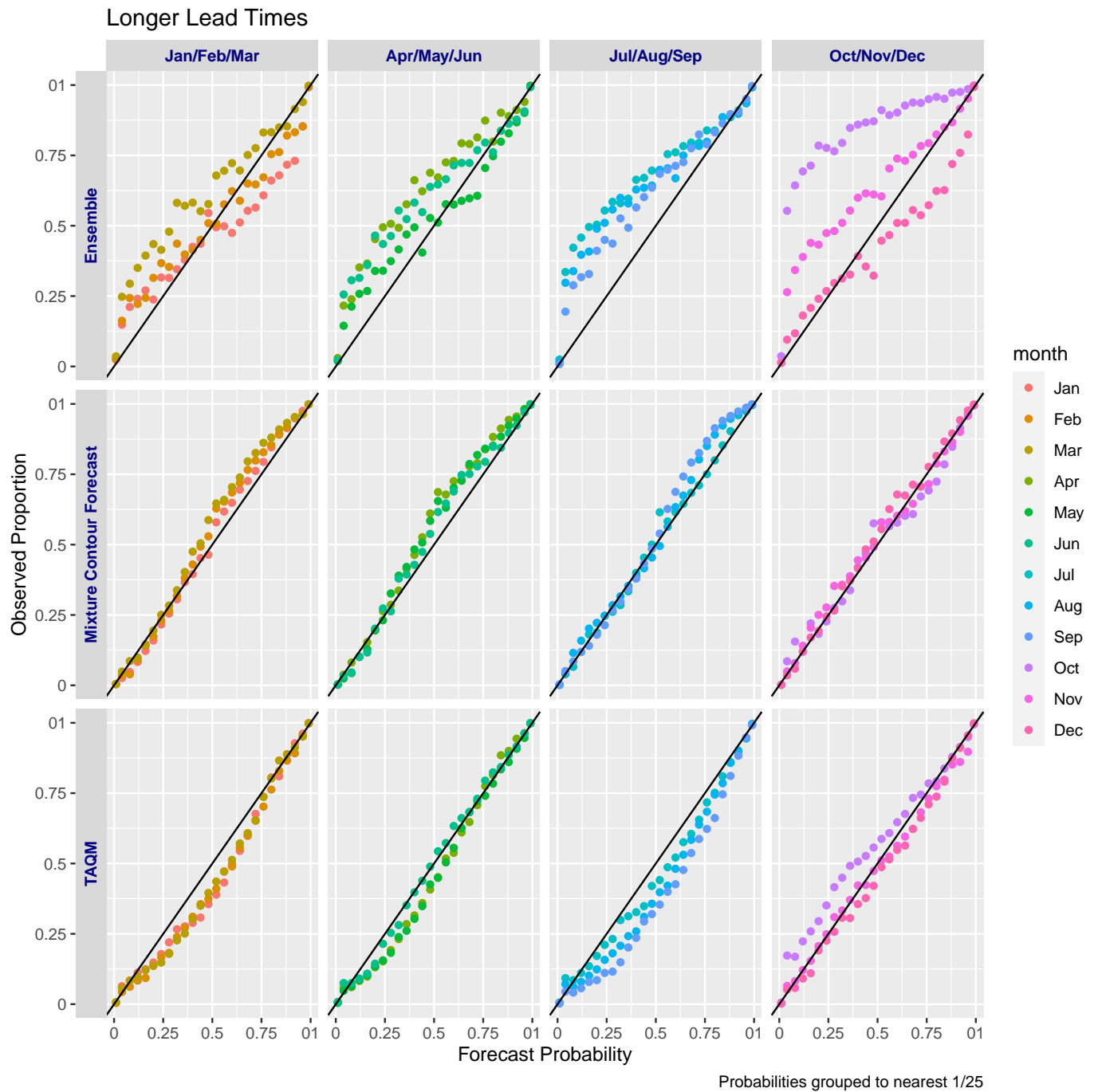


Figure 13: As in Figure 12 but for lead times of 2.5 - 6.5 months.

C MCMC diagnostics

As in all MCMC, diagnostic analysis is needed to determine the appropriate chain length. We selected the number iterations to run the sampler by considering traceplots and model diagnostics for sample forecast months. In this section, we evaluate one month in detail. Our analysis serves a dual purpose. It demonstrates that the number of iterations used in this paper’s analysis is reasonable and serves as a model for how MCMC diagnostics could be applied for future results obtained with this method.

We note that our primary goal in this paper is prediction and not inference and that only the mean of each parameter distribution is used. So, only reasonable sampling from the posterior distribution is needed for good performance. Therefore, we have not repeated this analysis on every forecast month and year. However, if our goals were to shift to inference on the parameter distributions, we would recommend doing a more thorough evaluation that would involve all parameters in each forecast month and year. We would also recommend repeating this initial diagnostic analysis if major changes are made to the method, such as changing the ensemble prediction system used in setting the hyperparameter μ_0 .

C.1 Example Evaluation: September 2005, 1.5-month lead

We evaluate the chains for September 2005 at a 1.5-month lead time using the training years of 1995-2004. We selected this month as an example, since the location of the sea ice edge is highly variable at this time of year. The model parameters are consequently likely to have high variability and need more iterations for fitting. Other months could potentially be fit adequately with less iterations.

Three regions contain sea ice in September 2005 and have a contour model fit for them: the Central Arctic, Baffin Bay, and the Greenland Sea. Using the *coda* R package (Plummer et al., 2006), we compute the Raftery and Lewis Diagnostic for κ and most values of μ_i and σ_i (Raftery and Lewis, 1992, 1995). We use $r = 0.0125$ and report the maximum number of iterations needed after assessing both $q = 0.025$ and $q = 0.975$. In Table 2 and Table 3, we report the 50-th, 95-th, and 100-th percentiles of the estimated number of iterations needed from all μ_i and σ_i for each region. We omit from this analysis some chains for σ_i and μ_i when more than 95% of the samples are within .05 of one of its boundaries (i.e., the upper or lower bound of the corresponding uniform prior as defined in Section 2.5 and Section 2.6 of the main text.) This omission, or something similar, is needed because in some cases the parameter value that maximizes the posterior is on the boundary of the range. The chain will correctly not move or move little in such cases and the Raftery and Lewis Diagnostic

does not make sense. In Table 4, we report the estimated number of iterations needed for κ for the three regions.

Table 2: The 50-th, 95-th, and 100-th percentile for the estimated chain lengths for μ_i obtained from the Raftery and Lewis Diagnostic for the three regions evaluated. Values rounded to the nearest whole number.

Region	$n_{est,50}$	$n_{est,95}$	$n_{est,100}$
Central Arctic	5820	10972	12715
Baffin Bay	3840	5414	5489
Greenland Sea	3829	8704	8884

Table 3: As in Table 2, except for σ_i

Region	$n_{est,50}$	$n_{est,95}$	$n_{est,100}$
Central Arctic	5380	10745	11520
Baffin Bay	5397	6182	6216
Greenland Sea	7345	15540	16533

Table 4: Estimated chain lengths from the Raftery and Lewis Diagnostic for κ

Region	n_κ
Central Arctic	3856
Baffin Bay	46544
Greenland Sea	36060

In Figure 14, we show the traceplot for a typical chain for μ_i for each of the three regions. Figure 15 is an analogous figure for a typical σ_i . We selected the index i plotted in each case by finding the chain with the estimated sample size closest to the median estimated number of iterations needed for all indices. Finally, Figure 16 shows the traceplots for κ for the three regions.

The traceplots illustrate that the chains converge quickly. The κ_i parameter tends to sample the space most slowly, so κ controls the number of iterations needed. In particular, the maximal value from the Raftery and Lewis diagnostic is approximately 45,000. The traceplots show that a burn-in of 5000 is sufficient for the chains to have reached their posterior density region. These results motivate using 55,000 iterations for all chains in the paper with the initial 5000 iterations removed as burn-in.

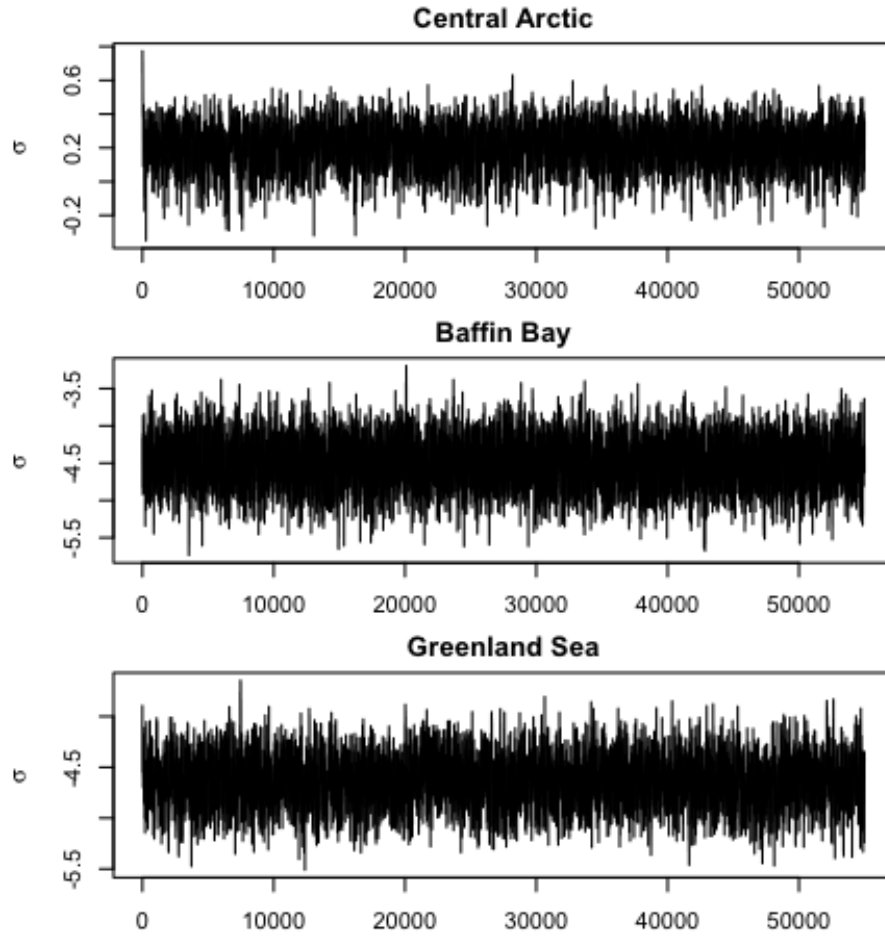


Figure 14: Traceplots for the chains in each of the three evaluated regions for a typical μ_i .

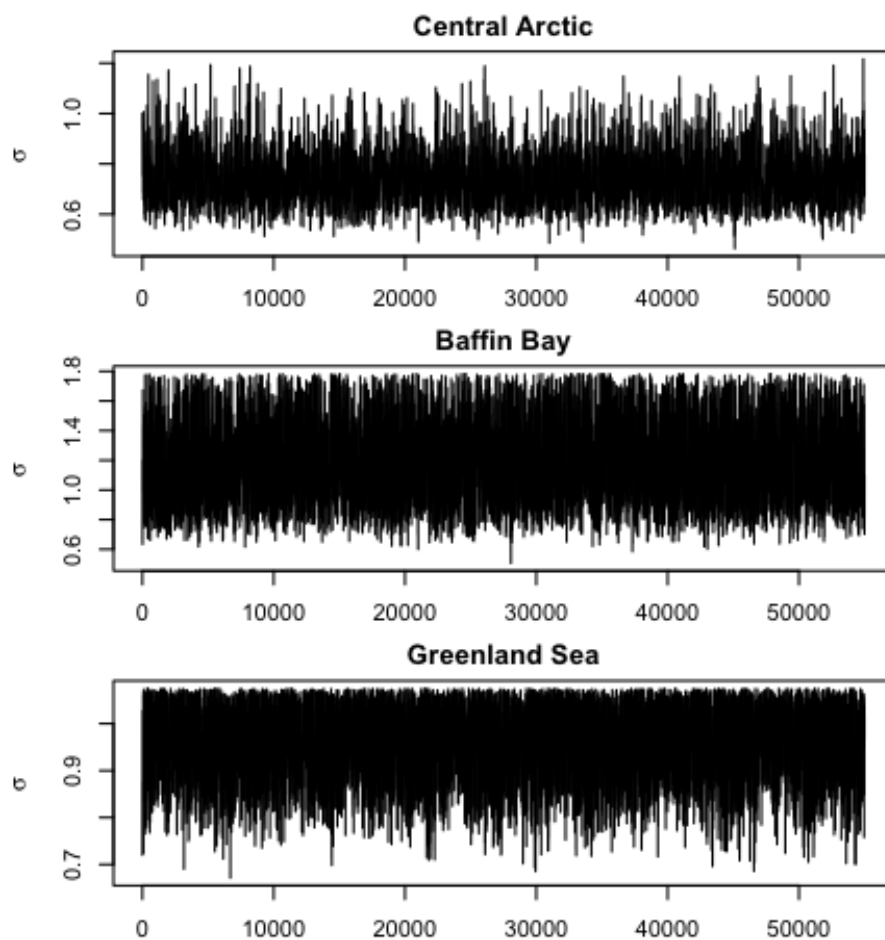


Figure 15: Traceplots for the chains in each of the three evaluated regions for a typical σ_i .

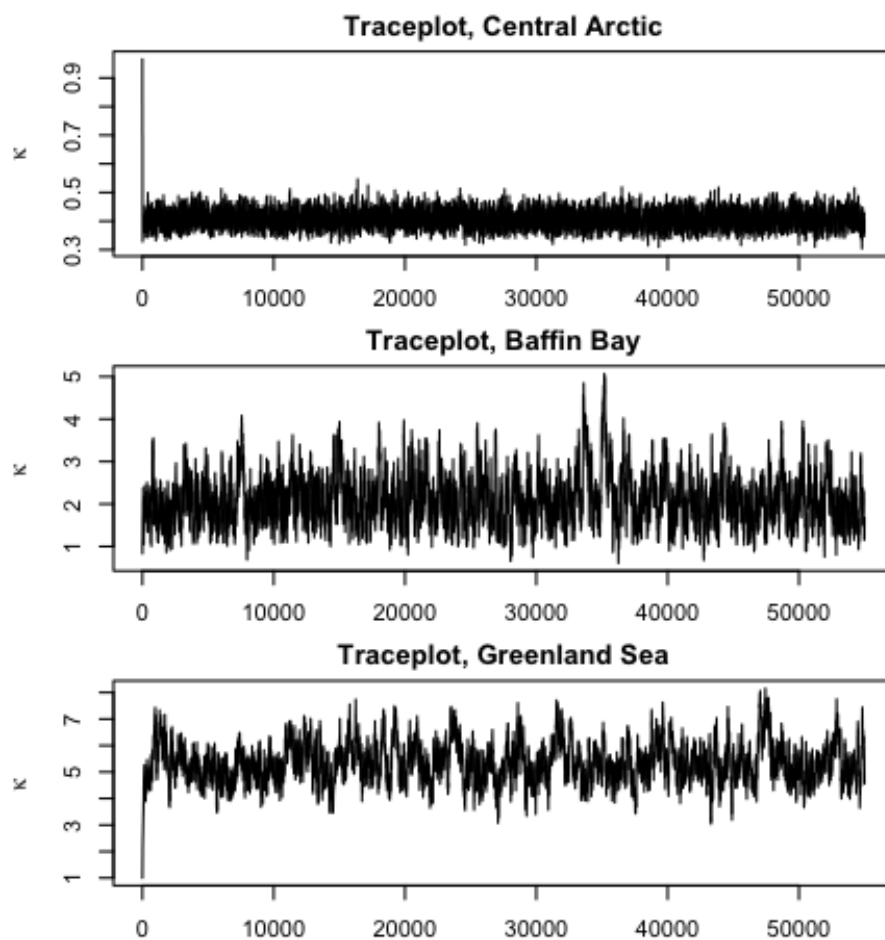


Figure 16: Traceplots for the parameter κ in the three evaluated regions.

D Length of Training Periods

Several aspects of the modeling in this paper rely on fitting parameters using multiple previous years of data as a training period. Since the Arctic is changing, more recent data is likely to be more relevant, but using only a small number of years of data may lead to parameter estimates that are too variable. Computational cost and limited amounts of data further constrain the training lengths possible. So, determining the appropriate training window length is not obvious. In this section, we discuss our rationale for the values used in the paper.

Because Contour-Shifting explicitly models the time trend, we follow Director et al. (2017) and use all available data prior to the forecast year to fit the bias correction. The earliest ensemble output ECMWF available on the Copernicus Climate Change Service Climate Data Store (Copernicus Climate Change Service, 2019) is for 1993, so that is the earliest year used in fitting Contour-Shifting.

The damped persistence forecast also relies on a trend. So, we use all available training data in fitting this reference forecast. Since this method only requires observations and they are available for earlier years than ensemble output, we fit this model with data beginning in 1981.

In the paper, we use only three years of training data in a rolling window to fit the weights in the mixture. Since the weights are dependent on results after post-processing, there is not enough data to do a proper cross validation while leaving aside a large enough test set. We find three years works well in practice, but it is not clear this is optimal. For future use, we evaluate the performance of different training lengths for the rolling window. We fit the weights and corresponding MCF forecasts for the years 2012-2016 using rolling windows of training lengths from 1-7 years. We report the mean Brier score over months and years. As in the main paper, we weight the grid boxes by their area. We find that a five-year training period performs best and would recommend this training length for operational use. We do note however that forecast performance does not appear to be particularly sensitive to this choice.

Table 5: Mean area-weighted Brier scores for MCF on the test set of 2012-2016 for different numbers of years of training data used to determine the weight on the climatology versus the contour model forecast.

Years	Mean Brier Score
1	0.03313
2	0.03317
3	0.03315
4	0.03293
5	0.03281
6	0.03286
7	0.03293